AD-A233 485

TECHNICAL REPORT BRL-TR-3204

BRL

AB INITIO STUDY OF THE ELECTRONIC MAGNETIC CIRCULAR DICHROISM SPECTRUM IN ACETYLENE: THE $\tilde{B} \leftarrow \tilde{X}$ AND $1^1B_2 \leftarrow \tilde{X}$ TRANSACTIONS

JAMES O. JENSEN
GEORGE F. ADAMS
CARY F. CHABALOWSKI

DTIC
MAR 1991

FEBRUARY 1991

U.S. ARMY LABORATORY COMMAND

BALLISTIC RESEARCH LABORATORY
ABERDEEN PROVING GROUND, MARYLAND

91 3 21 049

NOTICES

REPORT DOCUMENTATION PAGE	Form Approved OMB No. 0704-0188

1. AGENCY USE ONLY (Leave blank)	2. REPORT DATE February 1991	3. REPORT TYPE AND DATES COVERED Final Jan 89 – Jun 90

4. TITLE AND SUBTITLE

Ab Initio Study of the Electronic Magnetic Circular Dichroism Spectrum in Acetylene: The $\tilde{B}\leftarrow\tilde{X}$ and $1^1B_2\leftarrow\tilde{X}$ Transactions

5. FUNDING NUMBERS

1L161102AH43

6. AUTHOR(S)

James O. Jensen, George F. Adams, and Cary F. Chabalowski

7. PERFORMING ORGANIZATION NAME(S) AND ADDRESS(ES)

8. PERFORMING ORGANIZATION REPORT NUMBER

9. SPONSORING / MONITORING AGENCY NAME(S) AND ADDRESS(ES)

US Army Ballistic Research Laboratory
ATTN: SLCBR-DD-T
Aberdeen Proving Ground, MD 21005-5066

10. SPONSORING / MONITORING AGENCY REPORT NUMBER

BRL-TR-3204

12a. DISTRIBUTION / AVAILABILITY STATEMENT

Approved for public release;
distribution unlimited.

12b. DISTRIBUTION CODE

13. ABSTRACT (Maximum 200 words)

This study utilizes a newly implemented method based on first-order perturbation theory for calculating a priori, the electronic magnetic circular dichroism (MCD) spectra in molecules. As an initial application, the MCD band maxima have been calculated for the $\tilde{B}(1^1B_u)\leftarrow\tilde{X}(1^1A_g)$ and $1^1B_2\leftarrow\tilde{X}(1^1A_1)$ electronic transitions in the trans- and cis-bent conformations, respectively, of acetylene. The band intensity is assumed to come entirely from the $\mathcal{B}_o$-term in the MCD equations of Stephens, which explicitly includes a first-order perturbation correction to the two electronic states involved in the transition. The wavefunctions are determined using ab initio quantum chemical techniques including state-averaged CASSCF and multireference CI. There has been speculation that the $1^1B_2\leftarrow\tilde{X}$ band system might overlap the $\tilde{B}\leftarrow\tilde{X}$ and be part of the reason for the diffuse nature of the spectrum in the 185-170 nm region. This study considers this claim. The current calculations predict MCD band maxima for the 0-0 and 1-0 vibrational bands in the $\tilde{B}\leftarrow\tilde{X}$ to be $\Delta\varepsilon_o^{max}=-3.48$ and -5.82, respectively, while the experiment gives -0.8 and -1.6. This is 10^3 times larger than the largest band maximum ($\Delta\varepsilon_o^{max}(3-0)=-.0037$) calculated for the $^1B_2\leftarrow\tilde{X}$ transition. This study also finds the absorption oscillator strengths for the $\tilde{B}\leftarrow\tilde{X}$ to be a factor of 60 larger than that found in the $^1B_2\leftarrow\tilde{X}$. Thus, while these results do predict both the $\tilde{B}\leftarrow\tilde{X}$ and $1^1B_2\leftarrow\tilde{X}$ transitions to lie in the same spectral region, they do not support the hypothesis that the $1^1B_2\leftarrow\tilde{X}$ is a major contributor to either the absorption or MCD intensity in the 185–170-nm region.

14. SUBJECT TERMS

Acetylene, Electronic Absorption Spectrum, Magnetic Circular Dichroism Spectrum, Electronic States

15. NUMBER OF PAGES

51

16. PRICE CODE

17. SECURITY CLASSIFICATION OF REPORT	18. SECURITY CLASSIFICATION OF THIS PAGE	19. SECURITY CLASSIFICATION OF ABSTRACT	20. LIMITATION OF ABSTRACT
UNCLASSIFIED	UNCLASSIFIED	UNCLASSIFIED	UL

INTENTIONALLY LEFT BLANK.

TABLE OF CONTENTS

INTENTIONALLY LEFT BLANK.

LIST OF FIGURES

INTENTIONALLY LEFT BLANK.

LIST OF TABLES

INTENTIONALLY LEFT BLANK.

ACKNOWLEDGMENTS

INTENTIONALLY LEFT BLANK.

1. INTRODUCTION

In the preceding paper (Jensen, Adams, and Chabalowski, to be published) (Referred to as Report I) we reported *ab initio* calculations predicting the magnetic circular dichroism (MCD) spectra for the $\tilde{C} \leftarrow \tilde{X}$ transition in acetylene. In this second paper on MCD, we report on a new application of a recently implemented method for studying electronic spectral properties which exist due to interactions (perturbations) of the electronic state Ψ_A with a manifold of electronic states (Ψ_J's, with J≠A). This type of intensity borrowing is fundamental to the $\mathcal{B}_0$-term found in the general expression for the MCD intensity. In this study, we apply this new methodology to the *a priori* calculation of MCD spectra, again in the acetylene molecule, but for the spectral region 185-170 nm. The method is based on first-order perturbation theory and has been used successfully to study spin-orbit and spin-spin interactions in other molecules (Havriliak and Yarkony 1985; Chabalowski et al. 1989).

Gedanken and Schnepp (1976) have published the experimental electronic absorption and MCD spectra for acetylene in the spectral region 190-170 nm. They did not attempt to make an assignment or further explain the structure of a band system occurring in this region. Other experimental studies (Ingold and King 1953; King and Ingold 1952; Lassettre et al. 1968; Dance and Walker 1973; Foo and Innes 1973) have added strong evidence to the onset of a new band system near 185 nm, with the primary assignment of these spectra to the singlet $\tilde{B} \leftarrow \tilde{X}$ transition, with $\tilde{B}$ taken as the 1^1B_u state in the C_{2h} point group for a trans-bent (planar) conformation. Figure 1 shows the symmetry of the states arising from splitting the doubly degenerate $1^1\Delta_u$ state (linear conformation) by bending into the trans and cis-conformations. The spectrum beginning at 185 nm is reported to be "complicated" and "diffuse" (Gedanken and Schnepp 1976), due perhaps to some overlap by other electronic transitions as well as vibrational coupling of the $\tilde{B}$ to other electronic states (Peric, Buenker, and Peyerimhoff 1984). This is consistent with the experiment of Foo and Innes (1973) who have assigned high-lying vibrational bands of the $\tilde{A}(^1A_u) \leftarrow \tilde{X}$ transition at energies near the 0-0 of the $\tilde{B} \leftarrow \tilde{X}$

Theoretical studies have been carried out on several singlet electronic states in acetylene (Peric, Peyerimhoff, and Buenker 1985, 1987; Peric, Buenker, and Peyerimhoff 1984; Kammer 1970, 1974; Lischka and Karpfen 1986; So, Wetmore, and Schaefer 1980) and segments of the theoretically predicted potential energy surfaces (PES) were presented for these states (Peric, Peyerimhoff, and Buenker 1987; Kammer 1970). The results of the theoretical work support the assignment of at least part of the intensity in the spectral region 185-170 nm to the 1^1B_u state, and this assignment now

seems well accepted. The theory also suggests that the $1^1B_2 \leftarrow \tilde{X}$ transition could fall within this spectral region, causing part of the irregularities seen in the spectra.

Since only singlet electronic states are treated in this study, the spin multiplicity will be dropped from the state labels. The $\tilde{B}$ (B_u) state is the partner to the $2A_u$ state which arises from splitting the $1\Delta_u$ state by a planar trans-bending motion of the hydrogens (see Figure 1). The $\tilde{B}$ state shows a minimum in its PES near a $140°$ bend angle of the C-C-H with the linear conformation taken as $180°$. Because the $\tilde{B}$ state is not degenerate near its equilibrium point, it will be assumed that the MCD intensity arises from the $\mathcal{B}_0$-term which requires the use of non-degenerate perturbation theory to account for the intensity borrowing from other electronic states through magnetic dipole interactions. The $\tilde{B} \leftarrow \tilde{X}$ transition will, therefore, be treated using the newly implemented first-order perturbation techniques mentioned above. The $2A_u$ state is predicted to be linear (Peric, Peyerimhoff, and Buenker 1987; Peric, Buenker, and Peyerimhoff 1984; Kammer 1970; So, Wetmore, and Schaefer 1980) if the molecule is kept planar. However, earlier configuration interaction (CI) calculations show that the $2A_u$ state correlates with the 3^1A state in C_2 symmetry, and the 3^1A has a bent and twisted (about the C-C bond) minimum energy structure (Peric, Peyerimhoff, and Buenker 1987). So excitation into the $2A_u$ state should result in a bent and non-planar structure of C_2 symmetry.

Transition energies, absorption, and MCD intensities will also be calculated for the $1B_2 \leftarrow \tilde{X}$ band system in order to consider the possibility of this transition contributing to the spectra in the 185-170 nm region. The $1B_2$ arises from the cis-bending which splits the $1\Delta_u$ (Figure 1) into $1B_2$ and $2A_2$ in the C_{2v} point group, with the $1B_2$ predicted to have a non-linear (but planar) equilibrium geometry at a bend angle near $130°$ (Peric, Peyerimhoff, and Buenker 1987; Peric, Buenker, and Peyerimhoff 1984; Kammer 1970; So, Wetmore, and Schaefer 1980). The $2A_2$ (like the $2A_u$ of the trans-bent) correlates with the 3^1A state in C_2 and the same comments apply to its minimum energy structure (vide supra). For a comprehensive review of the singlet electronic states in acetylene, the reader is referred to the paper by Peric, Peyerimhoff, and Buenker (1987).

The *ab initio* wavefunctions will be developed from large atomic Gaussian basis sets and state-averaged multiconfiguration self-consistent field (MCSCF)/CI.
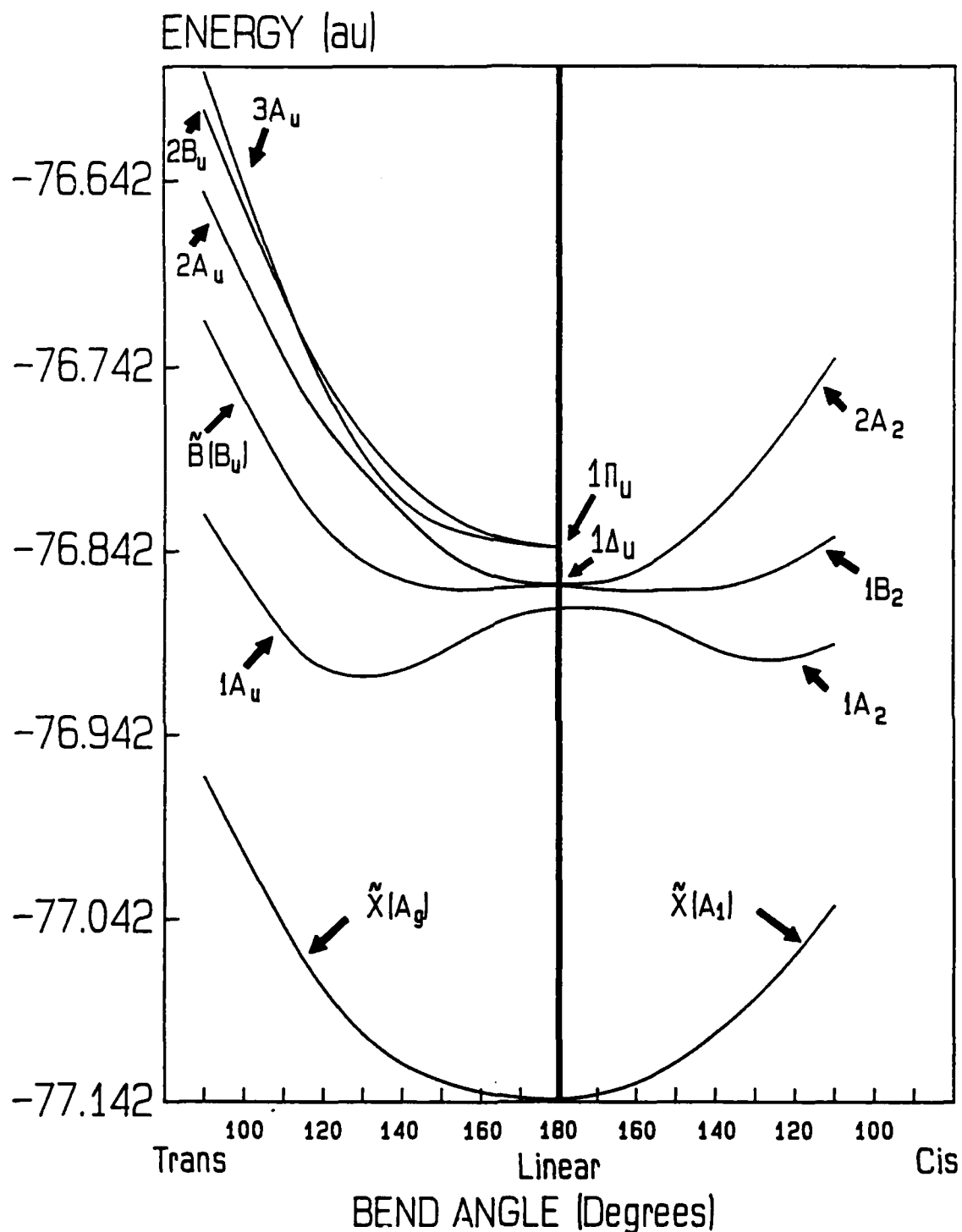
Figure 1. <u>Potential Energy Curves Calculated in this Study as a Function of Bend Angle (Using Ground State Bondlengths) for Low-Lying Singlet States in Acetylene. The Point Groups for the Cis- and Trans-conformations are C_{2v} and C_{2h}, Respectively</u>.

2. METHODS

State-averaged, complete active space MCSCF (SA-CASSCF) was performed for several electronic states at each point on the PESs and the resulting molecular orbitals (MO) were used as expansion vectors in the CIs. The CI wavefunctions were constructed in the space of all single and double excitations from a set of reference configuration state functions (CSF). Information on the SA-CASSCF and CI procedures used to obtain the zeroth-order wavefunctions was presented in Report I and will not be repeated here. Details of their applications to this study will be presented in the appropriate sections. For the sake of clarity, the general MCD equations and the details of the MCD $\overline{\mathcal{A}}$-term are presented here, as are the perturbation theory treatment of the $\overline{\mathcal{B}}$-term, and the equations needed to fit the MCD band maxima, denoted $\Delta \varepsilon_o^{max}$.

2.1 <u>MCD Equations</u>. The MCD intensity is given by the difference between the decadic molar extinction coefficients for left and right circularly polarized light, i.e., $\Delta \varepsilon = \varepsilon_L - \varepsilon_R$, (Stephens 1976; Piepho and Schatz 1983) and for a transition involving a non-degenerate ground state, $\widetilde{X}$, and a possible degenerate excited state, $\widetilde{I}$, we get

$$\frac{\Delta \varepsilon}{\overline{\upsilon}} = 653.2 \; \mu_B \left[\overline{A}_1 \left(\frac{\partial f}{\partial E} \right) + \overline{B}_o f \right] \cdot \overrightarrow{H} \tag{1}$$

where $\overline{\upsilon}$ is energy, f a line shape function, $\overrightarrow{H}$ the magnetic field in Gauss, and μ_B the Bohr magneton ($.4669 \times 10^{-4} cm^{-1}$/Gauss). $\overline{\mathcal{A}}_1$ and $\overline{\mathcal{B}}_o$ are given by

$$\overline{A}_1 = \frac{Im}{3} \sum_{\lambda, \lambda'} [< \overline{I}_\lambda | \overrightarrow{\mu} | \overline{I}_{\lambda'} > \cdot (< \overline{X} | \overrightarrow{m} | \overline{I}_\lambda > \times < \overline{I}_{\lambda'} | \overrightarrow{m} | \widetilde{X} >)] \tag{2}$$

4

$$\vec{B}_o = \frac{2Im}{3}\sum_\lambda \left[\sum_{J_k \neq X} \frac{<\vec{J}_k|\vec{\mu}|\vec{X}>}{E_{J_k}-E_X} \cdot \left(<\vec{X}|\vec{m}|\vec{I}_\lambda> \times <\vec{I}_\lambda|\vec{m}|\vec{J}_k>\right) \right.$$

$$\left. + \sum_{J_k \neq I_\lambda} \frac{<\vec{I}_\lambda|\vec{\mu}|\vec{J}_k>}{E_{J_k}-E_{I_\lambda}} \cdot \left(<\vec{X}|\vec{m}|\vec{I}_\lambda> \times <\vec{J}_k|\vec{m}|\vec{X}>\right) \right] \qquad (3)$$

with $\bar{\mu}$ and $\vec{m}$ being the magnetic and electric dipole moment operators. Equations 2 and 3 take into account the fact that the molecules are randomly oriented. The units are cgs with energies in cm^{-1}, electric dipole moments in Debye, and the magnetic field in Gauss. The operator, $\vec{m}$, is chosen in the length form, and the magnetic dipole moment operator, $\vec{\mu}$, is related to the orbital angular momentum operator, $\vec{L}$, by $\vec{\mu}=(1/2)\vec{L}$. The two operators are identical (in atomic units) except for the factor of 1/2.*

As Equation 2 is written, one sees that the $\bar{\mathcal{A}}_1$ term is derived for a truly degenerate excited state, $\tilde{I}$, and that a MCD band attributed to such a state will exhibit a characteristic derivative line shape. In

---

* The actual expression representing the $\Delta\varepsilon/E$ calculated in this study is given by

$$\frac{\Delta\varepsilon}{\bar{\upsilon}} = .01525\left[\bar{A}_1\left(\frac{\partial f}{\partial E}\right) + \bar{B}_o f\right]\cdot \vec{H}$$

which differs from Equation 1 in the units conversion due to the substitution of the orbital angular momentum operator for the magnetic dipole moment operator and carrying through the multiplication by μ_β, the Bohr magneton. The definitions of $\bar{\mathcal{A}}_1$ and $\bar{\mathcal{B}}_o$ then become

$$\bar{A}_1 = \frac{Im}{3}\sum_{\lambda,\lambda'}\cdot\left[<\vec{I}_\lambda|\vec{L}|\vec{I}_{\lambda'}> \cdot \left(<\vec{X}|\vec{m}|\vec{I}_\lambda> \times <\vec{I}_{\lambda'}|\vec{m}|\vec{X}>\right)\right]$$

$$\bar{B}_o = \frac{2Im}{3}\sum_\lambda\left[\sum_{J_k \neq X}\frac{<\vec{J}_k|\vec{L}|X>}{E_{J_k}-E_X}\cdot\left(<\vec{X}|\vec{m}|\vec{I}_\lambda> \times <\vec{I}_\lambda|\vec{m}|\vec{J}_k>\right)\right.$$

$$\left. + \sum_{J_k \neq I_\lambda}\frac{<\vec{I}_\lambda|\vec{L}|\vec{J}_k>}{E_{J_k}-E_{I_\lambda}}\cdot\left(<\vec{X}|\vec{m}|\vec{I}_\lambda> \times <\vec{J}_k|\vec{m}|X>\right)\right].$$

where use has been made of the relationship $\vec{\mu}=(1/2)\vec{L}$. The matrix elements,

$<\vec{I}_\lambda|\vec{L}|\vec{I}_{\lambda'}>$, $<\vec{J}_k|\vec{L}|\vec{X}>$, and $<\vec{I}_\lambda|\vec{L}|\vec{J}_k>$ come directly from the quantum chemical calculations.

contrast, the $\overline{\mathcal{B}}$-term can, in general, be non-zero for any electronic transition and will have the simple line shape of an absorption band. These line shape differences are often used to determine if a band involves a transition to a degenerate excited state. It should be pointed out that the $\overline{\mathcal{B}}$-term clearly contains the form of a first-order perturbation; i.e., $\tilde{X}$ and $\tilde{I}$ states are perturbed by a manifold of $\tilde{J}$ states via the magnetic dipole moment operator. For perturbations to the $\tilde{I}$ state:

$$\Psi_{I_\lambda}^1 = \sum_{J_k \neq I_\lambda} \frac{<I_\lambda | \vec{\mu} | J_\kappa>}{E_{J_k} - E_{I_\lambda}} \cdot <J_\kappa | . \tag{4}$$

The reader is referred to Stephens (1976) and Piepho and Schatz (1983) for detailed discussions of MCD theory, applications, and band shapes.

In order to relate the observed spectra to our theoretical results, we use a normalized Gaussian as our line shape function:

$$f = \frac{1}{\Delta (\Pi)^{1/2}} e^{-(\bar{\upsilon} - \bar{\upsilon}_o)^2 / \Delta^2} \tag{5}$$

$$f' = \frac{-2(\bar{\upsilon} - \bar{\upsilon}_o)}{\Delta^3 (\Pi)^{1/2}} e^{-(\bar{\upsilon} - \bar{\upsilon}_o)^2 / \Delta^2}. \tag{6}$$

The Δ is one-half the bandwidth measured at the band height of (f_{max}/e) and generally taken from the absorption spectrum. The transition energy in wavenumbers is $\bar{\upsilon}$ and $\bar{\upsilon}_o$ is the transition energy at the band maximum. Due to the lack of a baseline in the absorption spectrum of Gedanken and Schnepp, rough estimates of the bandwidths were taken from the MCD spectrum of Gedanken and Schnepp.

6

The oscillator strength for absorption from state $\bar{X}$ to state $\tilde{I}$ is defined as

$$f_{abs} = \frac{2}{3}\Delta E\,(au)\,|<\bar{X}\,|\,\vec{m}\,|\,\tilde{I}>|^2 \tag{7}$$

where ΔE is the transition energy and all quantities are in atomic units.

2.2   <u>Perturbed Wavefunctions</u>. The perturbed wavefunction for state Ψ_I is given through first-order in perturbation theory by

$$\Psi_I = \Psi_I^o + \Psi_I^1 \tag{8}$$

with Ψ_I^o being the zeroth-order approximation. The usual spectral representation for the first-order correction, Ψ_I^1, due to magnetic dipole interactions would be

$$\Psi_I^1 = \sum_{J\neq I}^{L} \frac{<\Psi_J^o\,|\,\vec{\mu}\,|\,\Psi_I^o>}{(E_I^o-E_J^o)}\,\Psi_J^o. \tag{9}$$

The summation over the L electronic states is, in principle, infinite. One often used approach to solving for Ψ_I^1 is to calculate explicitly the wavefunctions for a relatively small number of excited states, thereby drastically truncating L. This might cause one to miss important contributions to Ψ_I^1 from the omitted states.

Within a given CSF space, this "omitted states" problem is eliminated by solving for Ψ_I^1 directly from (Havriliak and Yarkony 1985)

$$(H^o-E)\Psi_I^1 = -\mu\Psi_I^o. \tag{10}$$

Equation 10 can be transformed into matrix form as

$$(\underline{H}^o-E)\underline{V}^I = -\underline{\mu}\underline{c}^I \tag{11}$$

where it must be emphasized that $\underset{\approx}{H}$ and $\underset{\approx}{\mu}$ matrices with elements formed over CSFs, not over eigenstates. The vectors $\underset{\sim}{V}$ and $\underset{\sim}{C}$ are defined as the coefficients for the first- and zeroth-order parts of Ψ_1:

$$\Psi_I^0 = \sum_i C_i^I \Psi_i(\kappa) \tag{12a}$$

$$\Psi_I^1 = \sum_j V_j^I \Psi_j(\kappa') . \tag{12b}$$

The κ and κ' label the spatial symmetries to which the CSFs belong, and, in general, $\kappa \neq \kappa'$. Equation 11 represents a large set of linear inhomogeneous equations which are solved to obtain $\underset{\sim}{V}$ by a variant of the method suggested by Pople, et al. (1979).

3. DETAILS OF CALCULATIONS

The basis set used is identical to that described in Report I, and consists of the primitives (11s, 7p) contracted to (5s, 4p) on the carbons and (6s) contracted to (3s) on the hydrogens. The carbon atoms were augmented with two uncontracted d-type polarization functions and the hydrogens each received one uncontracted p-type function. To the center of the C-C bond was added a set of (2s, 2p, 1d) uncontracted diffuse functions, thus giving a total of 84 atomic orbitals (AO), with the details given in Table 1 of Report I. The details of the SA-CASSCF and CI calculations will be presented in the sections discussing the electronic states.

Peric, Peyerimhoff, and Buenker (1987) have discussed many of the difficulties associated with studying the vibrational motions of the excited electronic states in acetylene, and particularly the $\tilde{B}$ state. Not the least of these difficulties is the probability of strong couplings amongst the bending and twisting modes. However, a treatment of the nuclear motion is required here because of a large difference in the equilibrium structures of the ground state and the $\tilde{B}$ and $1B_u$ states. A semi-quantitative treatment of the vibronic problem included in this study should be sufficient to address the electronic origin of the spectral features in the 185-170 nm range which is the goal of this work.

In this work, we employ a simplified treatment of the nuclear motion, ignoring all vibrational mode couplings (excepting the $2a_u$-$\tilde{B}$ over $\vec{\mu}$, to be discussed later) and keeping the C-C and C-H bond lengths fixed at the ground state values of R(C-C)=1.208Å and R(C-H)=1.058Å[20] for the calculation of transition moments. This choice of bond lengths was based upon the fact that we are predicting an absorption intensity from the ground state. The PESs for two states were then recalculated using the bond lengths determined by Peric, Peyerimhoff, and Buenker for the minimum energy structure of each state, these being the $\tilde{B}$[R(C-C)=1.349Å, R(C-H)=1.071Å] and $1B_2$[R(C-C)=1.351Å, R,(C-H)=1.104Å]. These PESs were then used in calculating a more appropriate set of vibrational wavefunctions. The PES for the $2A_u$ was uniformly lowered in energy by the energy difference for the $\tilde{B}$ state calculated at 180° using these two different sets of bond lengths. This was necessary to facilitate a more accurate coupling of the $\tilde{B}$ and $2A_u$ states.

The bending motions were described as a harmonic variation in the bending coordinate, θ, with θ given in radians. Due to the symmetry of the bending modes, the moments between the V"=0 (gerade) and all the odd numbered v' (ungerade) levels must integrate to zero over the electric dipole moment matrix elements. So the calculated vibrational levels describing the zero intensity moments will be removed and the remaining even states relabeled consecutively to correspond with the experimental notation.

Within the context of a single mode approximation it is necessary to assign a reduced mass for the mode in question. The reduced mass was obtained by fitting the calculated fundamental bending frequencies υ_4 (trans) and υ_5 (cis) to experiment for the $\tilde{X}$ and $\tilde{B}$, or to the calculated harmonic values of Lischka and Karpfen (1986) for the $2A_u$ state. This treatment is expected to be more reliable for the lower vibrational levels. The reduced masses for the trans-bending mode are calculated to be: ($\tilde{X}$:1.0), ($\tilde{B}$:0.73), and ($2A_u$:0.57). The reduced masses for the cis-bending mode are: ($\tilde{X}$:1.8), ($1B_2$:1.3), and ($2A_2$:0.635).

Henceforth, all quantities shall be reported in atomic units unless otherwise stated. The trans-bent and cis-bent conformations are treated in the point groups C_{2h} and C_{2v}, respectively, and the correspondence of the irreducible representations (IRREP) amongst the three symmetries, $D_{\infty h}$, C_{2h}, and C_{2v}, is given in Table 1. $D_{\infty h}$ corresponds to the linear molecule and is included for explanatory purposes. The molecule lies in the xy plane in C_{2h} with the C-C bond collinear to the x-axis, and in C_{2v} the molecule is in the yz plane with the C-C collinear to the y-axis.

Table 1. Correspondence of Irreducible Representations for Acetylene in the Trans-bent C_{2h}, Linear $D_{\infty h}$, and Cis-bent C_{2v} Conformations

C_{2h}	$D_{\infty h}$	C_{2v}
A_g	Σ_g^+	A_1
A_u	Σ_u^-	A_2
A_u, B_u	Δ_u	A_2, B_2
A_u, B_u	Π_u	A_1, B_1
A_g, B_g	Π_g	A_2, B_2
A_g, B_g	Δ_g	A_1, B_1

3.1 The $\tilde{B} \leftarrow \tilde{X}$ Transition; Trans-bend.

3.1.1 Zeroth-order State Descriptions. The trans-bend $\tilde{B}$ (B_u) state, which arises from the degenerate $1\Delta_u$, is represented by the CSFs $(1\sigma_g^2 1\sigma_u^2 2\sigma_g^2 2\sigma_u^2) 3\sigma_g^2 1\pi_{uy}^1 1\pi_{uz}^2 1\pi_{gy}^1$ and

$(\ldots) 3\sigma_g^2 1\pi_{uy}^2 1\pi_{uz}^1 1\pi_{gz}^1$. Its degenerate partner is the linear $2A_u$ and is given by the CSFs

$(\ldots) 3\sigma_g^2 1\pi_{uy}^1 1_{uz}^2 1\pi_{gz}^1$ and $(\ldots) 3\sigma_g^2 1\pi_{uy}^2 1\pi_{uz}^1 1\pi_{gy}^1$. The active orbitals used in the SA-CASSCF are the $3\sigma_g (4a_g), 1\pi_{gy}(5a_g), 1\pi_{uy}(3b_u), 1\pi_{uz}(1a_u), 1\pi_{gz}(1b_g)$ with the $4\pi_u$ electrons distributed amongst these MOs. The $3\sigma_g (4a_g)$ MO is a Rydberg orbital. Six electronic states were then averaged including $1A_g, 1,2B_u, 1,2,3A_u$. The weighting scheme used in the averaging is $w_k=(1,1,1,1,1,1)$, respectively. The SA-CASSCF was calculated at each point along the bending PES, which ranged from $180°$ (linear) to $110°$ at $10°$ increments, and another point at $90°$.

To test the effects of the choice of weights on the transition moments, a test was run at a bend angle of $150°$ using the new weights $w_k=(2,1,1,1,1,1)$. Only two of the transition moments changed more than 4%, and these two moments are relatively small and contribute to the total MCD intensity in such a way as to have changed the final intensity by less than 2%. These size fluctuations in the moments are quite in line with the expected accuracies for this study.

10

Reference CSFs were determined from preliminary CI calculations at 180° (linear) and 140°. The number of states included per IRREP are $3(A_g)$, $3(A_u)$, $2(B_u)$, and $3(B_g)$, and the contribution of the reference set to the wavefunction is given by c_{refs}^2:

$$c_{refs}^2 = \sum_{i}^{ref\,CSFs} c_i^2$$

where c_i^2 is the CI coefficient for the ith reference CSF in a given state. The CI results at both angles give $c_{refs}^2 \geq (.88, .90, .90, .88)$ for any state in the A_g, A_u, B_u, B_g IRREPS, respectively. And, for the states of primary interest, $c_{refs}^2 \geq \tilde{X}\,(.91)$, $2A_u\,(.91)$, $\tilde{B}\,(.90)$. The list of reference CSFs, and the total number of CSFs generated in each IRREP, are shown in Table 2. All the states mentioned above represent electronic excitations out of the $1\pi_{uy}(b_u)1\pi_{ux}(a_u)$ orbitals. The excited states of primary interest are obtained by excitations into the $1\pi_{gy}(a_g)1\pi_{gx}(b_g)$ orbitals. PESs for the lowest six singlet states are shown in Figure 1, and the data given explicitly in Table 3.

3.1.2 Perturbed Wavefunctions. The total perturbed wavefunctions, $\Psi(\tilde{X})$ and $\Psi(\tilde{B})$, arise from the magnetic dipole induced perturbations to the zeroth-order electronic state wavefunctions, $\Psi°(\tilde{X})$ and $\Psi°(\tilde{B})$, as given by

$$\Psi(\tilde{X}) = \Psi°(\tilde{X}) + \Psi^1(B_g^x;\tilde{X}) + \Psi^1(B_g^y;\tilde{X}) + \Psi^1(A_g^z;\tilde{X}) \tag{13a}$$

$$\Psi(\tilde{B}) = \Psi°(\tilde{B}) + \Psi^1(A_u^x;\tilde{B}) + \Psi^1(A_u^y;\tilde{B}) + \Psi^1(B_u^z;\tilde{B}) \tag{13b}$$

where the first-order corrections arise from the magnetic dipole interactions,

$$\Psi^1(B_g^x;\tilde{X}) : <B_g\,|\mu_x\,|\,\Psi°(\tilde{X})>$$

Table 2. Reference CSFs Used in Trans-bendng Conformations (C_{2h} Symmetry) and Total Number of CSFs Generated Per IRREP[a]

MO IRREP	$2a_g$	$3a_g$	$4a_g$	$5a_g$	$2b_u$	$3b_u$	$4b_u$	$5b_u$	$6b_u$	$7b_u$	$1a_u$	$1b_g$	$2b_g$
A_g	2	2	-	-	2	2	-	-	-	-	2	-	-
(271428)[b]	2	2	-	2	2	-	-	-	-	-	2	-	-
	2	2	-	-	2	2	-	-	-	-	-	2	-
	2	2	-	1	2	1	-	-	-	-	1	1	-
	2	2	-	-	2	1	1	-	-	-	2	-	-
	2	2	-	-	2	1	-	-	1	-	2	-	-
	2	2	-	-	2	1	-	1	-	-	2	-	-
	2	2	-	-	2	1	-	-	-	1	2	-	-
A_u	2	2	-	-	2	1	-	-	-	-	2	1	-
(186914)	2	2	1	-	2	2	-	-	-	-	1	-	-
	2	2	-	1	2	2	-	-	-	-	1	-	-
	2	2	-	-	2	1	-	-	-	-	2	-	1
	2	2	-	-	2	1	-	-	-	-	2	1	-
	2	2	1	2	2	-	-	-	-	-	1	-	-
Bg	2	2	-	-	2	2	1	-	-	-	1	-	-
(313910)	2	2	-	2	2	-	1	-	-	-	1	-	-
	2	2	-	-	2	2	-	-	1	-	1	-	-
	2	2	-	-	2	2	-	1	-	-	1	-	-
	2	2	-	1	2	1	1	-	-	-	-	1	-
	2	2	-	2	2	-	-	1	-	-	1	-	-
	2	2	-	-	2	2	-	-	-	1	1	-	-
B_u	2	2	-	-	2	2	-	-	-	-	1	1	-
(184782)	2	2	-	1	2	1	-	-	-	-	2	-	-
	2	2	1	-	2	1	-	-	-	-	2	-	-
	2	2	-	-	2	2	-	-	-	-	1	-	1
	2	2	1	-	2	1	-	-	-	-	-	2	-

[a] The $1a_g$ and $1b_u$ MOs, which correspond to the carbon inner shells, were treated as frozen core orbitals in the CI.
[b] Total number of CSFs actually included in the CI and properties calculations. See text for further details.

12

Table 3. State Energies vs. Bend Angle

Bend Angle	TRANS-ENERGIES				CIS-ENERGIES			
	A_s	A_s	B_s	$1B_1^a$	A_1	A_2	B_2	B_2^a
180	-77.14098	-76.87349 .86088 .84112	-76.86121 .84123	-76.87724	-77.14057	-76.87350 .86091	-76.86003	-76.87384
170	-77.14016	-76.87579 .86124 .83957	-76.86220 .83910	-76.87845	-77.13835	-76.87626 .86119	-76.86138	-76.87593
160	-77.13729	-76.88547 .85534 .83530	-76.86378 .83262	-76.88102	-77.13163	-76.88638 .85457	-76.86393	-76.88015
150	-77.13150	-76.89790 .84176 .82796	-76.86364 .82132	-76.88294	-77.12050	-76.89680 .84090	-76.86527	-76.88345
140	-77.12152	-76.90785 .82078 .81633	-76.85947 .80424	-76.88176	-77.10518	-76.90259 .82168	-76.86363	-76.88313
130	-77.10556	-76.91199 .79907 .79147	-76.84905 .78019	-76.87503	-77.08587	-76.90181 .79771	-76.85823	-76.87931
120	-77.08138	-76.90763 .77392 .75319	-76.83035 .74791	-76.86035	-77.06281	-76.89341 .76970	-76.84895	-76.87200

13

Table 3. State Energies vs. Bend Angle (Continued)

Bend Angle	TRANS-ENERGIES				CIS-ENERGIES			
	A_g	A_u	B_u	$1B_u^a$	A_1	A_2	B_2	B_u^a
110	-77.04824	-76.89228 .73975 .70484	-76.80156 .70656	-76.83533	-77.03525	-76.87591 .73804	-76.83533	-76.86148
90	-77.96495	-76.82193 .64828 .58340	-76.71727 .60356	-76.75027	b	b	b	-76.82483

[a] These energies have been re-calculated using the bond lengths for the minimum energy structure in this state (Peric, Buenker, and Peyerimhoff 1984). All other calculations use the ground state bond lengths.
[b] This bend angle was not calculated, but determined by fit to parabola.

14

$$\Psi^1(B_g^y;\tilde{X}) \; : \; <B_g|\mu_y|\Psi^o(\tilde{X})>$$

$$\Psi^1(A_g^z;\tilde{X}) \; : \; <A_g|\mu_z|\Psi^o(\tilde{X})>$$

$$\Psi^1(A_u^x;\tilde{B}) \; : \; <A_u|\mu_x|\Psi^o(\tilde{B})>$$

$$\Psi^1(A_u^y;\tilde{B}) \; : \; <A_u|\mu_y|\Psi^o(\tilde{B})>$$

$$\Psi^1(B_u^z;\tilde{B}) \; : \; <B_u|\mu_z|\Psi^o(\tilde{B})>$$

and the matrix elements listed above are between zeroth-order wavefunctions for the $\tilde{X}$ or $\tilde{B}$ states and the manifold of states having the specified symmetry.

3.1.3 $\overline{\mathcal{B}}_o$ Over Perturbed Wavefunctions.

Expanding the cross products and dot products in Equation 3 and inserting the first-order corrections to the wavefunctions from Equation 13 gives $\overline{\mathcal{B}}_o^\dagger$

$$\overline{B}_o^\dagger = \frac{2Im}{3}\left[\left\{<\Psi^o(\tilde{X})|m_y|\Psi^o(\tilde{B})><\Psi^o(\tilde{B})|m_z|\Psi^1(B_g^x;\tilde{X})>\right.\right.$$

$$-<\Psi^o(\tilde{X})|m_x|\Psi^o(\tilde{B})><\Psi^o(\tilde{B})|m_z|\Psi^1(B_g^y;\tilde{X})>$$

$$+<\Psi^o(\tilde{X})|m_x|\Psi^o(\tilde{B})><\Psi^o(\tilde{B})|m_y|\Psi^1(A_g^z;\tilde{X})>$$

$$\left.-<\Psi^o(\tilde{X})|m_y|\Psi^o(\tilde{B})><\Psi^o(\tilde{B})|m_x|\Psi^1(A_g^z;\tilde{X})>\right\} \tag{14a}$$

$$-\left\{<\Psi^o(\tilde{X})|m_y|\Psi^o(\tilde{B})><\Psi^o(\tilde{X})|m_z|\Psi^1(A_u^x;\tilde{B})>\right.$$

$$-<\Psi^o(\tilde{X})|m_x|\Psi^o(\tilde{B})><\Psi^o(\tilde{X})|m_z|\Psi^1(A_u^y;\tilde{B})>$$

$$+<\Psi^o(\tilde{X})|m_x|\Psi^o(\tilde{B})><\Psi^o(\tilde{X})|m_y|\Psi^1(B_u^z;\tilde{B})>$$

$$\left.\left.-<\Psi^o(\tilde{X})|m_y|\Psi^o(\tilde{B})><\Psi^o(\tilde{X})|m_x|\Psi^1(B_u^z;\tilde{B})>\right\}\right] \tag{14b}$$

15

where the dagger on $\overline{\mathcal{B}}_o^{-\dagger}$ indicates that vibrational motion has been ignored in the electronic wavefunctions.

Finally, for each matrix element in Equation 14. we need to obtain the vibrationally-averaged electric transition dipole moment between two bound electronic states. For example, using the zeroth-order PESs to calculate the vibrational wavefunctions we get,

$$S(\tilde{X} \mid \tilde{B})^y_{v'v''} = <\chi^{\tilde{X}}_{v''}(R) \mid <\Psi^o(\tilde{X}) \mid m_y \mid \Psi^o(\tilde{B})> \mid \chi^{\tilde{B}}_{v'}(R)> \qquad (15a)$$

$$S(\tilde{B}) \mid (B^x_g; \tilde{X}))^z_{v'v''} = <\chi^{\tilde{B}}_{v'}(R) \mid <\Psi^o(\tilde{B}) \mid m_z \mid \Psi^1(B^x_g; \tilde{X})> \mid \chi^{\tilde{X}}_{v''}(R)> . \qquad (15b)$$

The vibrational wavefunctions, χ_v (R)'s, are obtained by numerically solving the vibrational Schroedinger equation for nuclear motion while ignoring rotational effects. The integrals in Equations 15a and 15b are then solved numerically using Simpson's rule.

The final form for $\overline{\mathcal{B}}_o$, which includes vibrational averaging, is

$$\overline{B}_o = \frac{2Im}{3} \left[\left\{ S(\tilde{X} \mid \tilde{B})^y_{v'v''} \cdot S(\tilde{B} \mid (B^x_g; \tilde{X}))^z_{v'v''} - S(\tilde{X} \mid \tilde{B})^x_{v'v''} \cdot S(\tilde{B} \mid (B^y_g; \tilde{X}))^z_{v'v''} \right. \right.$$

$$+ S(\tilde{X} \mid \tilde{B})^z_{v'v''} \cdot S(\tilde{B} \mid (A^x_g; \tilde{X}))^y_{v'v''} - S(\tilde{X} \mid \tilde{B})^z_{v'v''} \cdot S(\tilde{B} \mid (A^y_g; \tilde{X}))^x_{v'v''} \right\}$$

$$- \left\{ S(\tilde{X} \mid \tilde{B})^y_{v'v''} \cdot S(\tilde{X} \mid (A^x_u; \tilde{B}))^z_{v'v''} - S(\tilde{X} \mid \tilde{B})^x_{v'v''} \cdot S(\tilde{X} \mid (A^y_u; \tilde{B}))^z_{v'v''} \right.$$

$$\left. \left. + S(\tilde{X} \mid \tilde{B})^z_{v'v'} \cdot S(\tilde{X} \mid (B^x_u; \tilde{B}))^y_{v'v''} - S(\tilde{X} \mid; \tilde{B})^y_{v'v''} \cdot S(\tilde{X} \mid (B^z_u; \tilde{B}))^x_{v'v''} \right\} \right] \qquad (16)$$

3.1.4 Quasi-degenerate Perturbation Theory. The $\tilde{B}$ and $2A_u$ are degenerate at 180° (and nearly so for small bend angles); thus, the magnetic dipole interaction between these two states cannot be treated near the linear conformation using the non-degenerate perturbation theory outlined above. Instead, a quasi-degenerate perturbation scheme (Yarkony 1988) will be used in which the $\Psi(A_u)$ space is partitioned into two parts: a P space containing only the quasi-degenerate electronic state, $\Psi(2A_u)$ and a space containing all the remaining $\Psi(A_u)$ states. If we label the $\tilde{B}$ state as the I'th state, the wavefunction for $\tilde{B}$ becomes

16

$$\Psi^d(I) = \Psi^\circ(I) + \Psi_Q^1(J,I) \tag{17}$$

where Ψ^d is referred to as a dressed wavefunction, and Ψ_Q^1 is the dressing wavefunction. $\Psi_Q^1(J,I)$ is defined by

$$\Psi_Q^1(J,I) = \hat{Q}\Psi^1(J,I); \; with \; \hat{Q} = (1 - \sum_{J \varepsilon P(J)} | \Psi^\circ(J) >< \Psi^\circ(J) |) \tag{18}$$

with P(J) containing only the $2A_u$ element for the current case. $\Psi_Q^1(J,I)$ satisfies

$$(H^\circ - E)\Psi_Q^1(J,I) = \hat{Q}\mu\Psi^\circ(I) \tag{19}$$

with μ the magnetic dipole operator and $\hat{Q}$ the projection operator defined in Equation 18. Specifically, $\hat{Q}$ projects out the contribution of $\Psi^\circ(2A_u)$ from $\Psi^1(J,I)$ leaving the dressing function, $\Psi_Q^1(J,I)$, which contains the interaction of $\Psi^\circ(\tilde{B})$ with all other $\Psi^\circ(A_u)$ except the $\Psi^\circ(2A_u)$. Equation 19 is then solved directly in the CSF basis as discussed in Section 2.2.

We now want to include the interaction of the quasi-degenerate $\Psi^\circ(2A_u)$ with the $\Psi^\circ(\tilde{B})$ state over the magnetic dipole moment operator, μ. This is done by coupling the vibrational levels of the two electronic states to form new vibronic states, $\Psi_K(r,R)$ (Yarkony 1988):

$$\Psi_K(r,R) = \sum_{I,\lambda} d_{I\lambda}^K \chi_\lambda^I \Psi_I^d(r,R) \tag{20}$$

where I runs over the electronic wavefunctions for the two quasi-degenerate states. The $\chi_\lambda^I(R)$ satisfy

$$(\hat{T}_N + E_I^e(R))\chi_\lambda^I(R) = \chi_\lambda^I(R)\varepsilon_{I\lambda} \tag{21}$$

with

$$E_I^e(R) = <\Psi_I^d(r;R)|H^e|\Psi_I^d(r;R)>.$$

The $\Psi_K(r,R)$ satisfy the total (rotationless) Schroedinger equation,

$$(T_N + H^e)\Psi_K(r,R) = E_K\Psi_K(r,R),$$ (22)

where K is a coupled vibronic state formed as a linear combination of the vibrational levels of the $\Psi^\circ(2A_u)$ and $\Psi^\circ(\tilde{B})$ states with the coupling coefficients, $d_{I\lambda}^K$, determined from the relationships

$$(\varepsilon - E_\kappa)D^K = \Gamma D^K$$ (23)

with

$$\varepsilon_{I\lambda,I'\lambda'} = \delta_{I,I'}\delta_{\lambda,\lambda'}\varepsilon_{I\lambda},$$ (24)

$$\Gamma_{I\lambda,I'\lambda'} = <\chi_\lambda^I<\Psi_I^d \mid \vec{\mu} \mid \Psi_{I'}^d> \chi_{\lambda'}^{I'}>_R$$

$$= <\chi_\lambda^I \mid \underline{\mu}(I,I') \mid \chi_{\lambda'}^{I'}>_R \quad \text{if } I \neq I'$$

$$= 0 \qquad\qquad \text{if } I = I'.$$ (25)

The magnitude of the coupling coefficients is determined in part by the size of the magnetic dipole moment matrix element coupling the $2A_u$ and $\tilde{B}$ states. Based on the coupling coefficients, $d_{I\lambda}^K$, one can often assign the vibronic states, Ψ_K (r,R), as being composed primarily of $\Psi^\circ(2A_u)$ or $\Psi^\circ(\tilde{B})$. Making such an assignment becomes more meaningful when $|\varepsilon_{I\lambda} - \varepsilon_{I'\lambda'}| >> \Gamma_{I\lambda,I'\lambda'}$.

The contribution to the $\overline{\mathfrak{A}}$-term in Equation 16 through the matrix elements involving the vibronic wavefunctions, $\Psi_K(r,R)$, is given explicitly by

$$S(\bar{X} \mid (A_u^x;\bar{B}))_{v',v''}^z = <\chi_{v'}^{\bar{X}}(R) \mid <\Psi^\circ(\bar{X}) \mid m_z \mid \Psi_Q^1(A_u^x;\bar{B})> \mid \chi_{v''}^{\tilde{B}}(R)>$$

$$+ <\chi_{v'}^{\bar{X}}(R) \mid <\Psi^\circ(\bar{X}) \mid m_z \mid \Psi_K(r,R)>>.$$ (26)

18

From Equation 20, we find $\Psi_K(r,R)$ to be

$$\Psi_K(r,R) = \sum_\lambda d^K_{2A_u^z,\lambda}\, \chi^{2A_u}_\lambda(R)\Psi^o(2A_u) + \sum_\gamma d^K_{\bar{B},\gamma}\chi^{\bar{B}}_\gamma(R)\Psi^o(\bar{B}). \tag{27}$$

Substituting Equation 27 for Ψ_K into Equation 26 gives

$$S(\bar{X}\,|\,(A_u^z;\bar{B}))^{\prime}_{v',v''} = <\chi^{\bar{X}}_{v''}(R)\,|<\Psi^o(\bar{X})\,|\,m_z\,|\,\Psi^1_Q(A_u^z;\bar{B})>\,|\,\chi^{\bar{B}}_{v'}(R)>$$

$$+ \sum_\lambda d^K_{2A_z,\lambda}<\chi^{\bar{X}}_{v''}(R)\,|<\Psi^o(\bar{X})\,|\,m_z\,|\,\Psi^o(2A_u)>\,|\chi^{2A_u}_\lambda(R)> \tag{28}$$

$$+ \sum_\gamma d^K_{\bar{B},\gamma}<\chi^{\bar{X}}_{v''}(R)\,|<\Psi^o(\bar{X})\,|\,m_z\,\Psi^o(\bar{B})>\,|\,\chi^{\bar{B}}_\gamma(R)>.$$

where the superscript on the $2A_u$ in $d^k_{2A_z}$ indicates the coupling coefficient was determined using the x-component of the magnetic dipole moment. Based on symmetry arguments, the third term in Equation 28 is zero, giving the final expression

$$S(\bar{X}\,|\,A_u^z;\bar{B}))^{\prime}_{v',v''} = <\chi^{\bar{X}}_{v''}(R)\,|<\Psi^o(\bar{X})\,|\,m_z\,|\,\Psi^1_Q(A_u^z;\bar{B})>\,|\,\chi^{\bar{B}}_{v'}(R)>$$

$$+ \sum_\lambda d^K_{2A_z,\lambda}<\chi^{\bar{X}}_{v''}(R)\,|<\Psi^o(\bar{X})\,|\,m_z\,|\,\Psi^o(2A_u)>\,|\chi^{2A_u}_\lambda(R)>. \tag{29}$$

An analogous expression can be written for the $S(\bar{X}\,|\,(A_u^y;\bar{B}))^{\prime}_{v',v''}$ matrix element in Equation 16, with the coupling coefficients, $d^K_{2A_u^y,\lambda}$, being determined from the y-component of the magnetic dipole moment coupling matrix element.

3.2 $1^1B_2 \leftarrow \tilde{X}$ Transition; Cis-bend.

3.2.1 Zeroth-order State Descriptions. The cis-bent $1B_2$ state (in C_{2v} symmetry) comes from splitting the degenerate $1\Delta_u$ and is described (for the linear molecule) by the CSFs $(1\sigma^2_g 1\sigma^2_u 2\sigma^2_g 2\sigma^2_u)$ $3\sigma^2_g 1\pi^1_{ux} 1\pi^2_{uz} 1\pi^1_{gx}$ and $(...)3\sigma^2_g 1\pi^2_{ux} 1\pi^1_{uz} 1\pi^1_{gz}$. Its degenerate partner is the linear $2A_2$ and is given by the CSFs $(...)3\sigma^2_g 1\pi^1_{ux} 1\pi^2_{uz} 1\pi^1_{gz}$ and $(...)3\sigma^2_g 1\pi^2_{uy} 1\pi^1_{ux} 1\pi^1_{gx}$. The active orbitals used in the

distributed amongst these MOs. The $2\sigma_u(3b_2)$ MO is a Rydberg orbital. Six electronic states were then averaged including $1A_1$, $1,2B_2$, $1,2,3A_2$. The weighting scheme used in the averaging is $w_k=(1,1,1,1,1,1)$, respectively. The SA-CASSCF was calculated at each point along the bending PES, which ranged from $180°$ (linear) to $110°$ at $10°$ increments.

Analogous to the trans-bent case, the reference CSFs were determined by running CIs at cis-bend angles of $180°$ (linear) and $140°$. The number of states included per IRREP were $3(A_1)$, $3(A_2)$, $2(B_1)$, and $2(B_2)$. At both angles, the total contribution of the reference set to the wavefunctions in each IRREP are $c^2_{refs} \geq (.88, .91, .89, .90)$, respectively, and, for the states of primary interest, $c^2_{refs} \geq \tilde{X}(A_1)(.92)$, $1B_2(.90)$. The list of reference CSFs and the total number of CSFs generated in each IRREP are shown in Table 4. All the states mentioned above represent electronic excitations out of the $1\pi_{ux}(b_1)1\pi_{uz}(a_1)$ orbitals. The excited state of primary interest here is the $1B_2$. This is obtained by excitations into the $1\pi_{gx}(a_2)1\pi_{gz}(b_2)$ orbitals. The resulting PESs for the lowest four singlet states are shown in Figure 1 and the data given explicitly in Table 3.

3.2.2 Perturbed Wavefunctions.

The perturbed wavefunctions $\Psi(\tilde{X})$ and $\Psi(1B_2)$ may be written as

$$\Psi(\tilde{X}) = \Psi^\circ(\tilde{X}) + \Psi^1(B_2^x;\tilde{X}) + \Psi^1(A_2^z;\tilde{X}) \qquad (30a)$$

$$\Psi(1B_2) = \Psi^\circ(1B_2) + \Psi^1(A_1^x;1B_2) + \Psi^1(B_1^z;1B_2) \qquad (30b)$$

where the first-order corrections arise from the magnetic dipole interactions

$$\Psi^1(B_2^x;\tilde{X}) : <B_2 | \mu_x | \Psi^\circ(\tilde{X})>$$

$$\Psi^1(A_2^z;\tilde{X}) : <A_2 | \mu_z | \Psi^\circ(\tilde{X})>$$

$$\Psi^1(A_1^x;1B_2) : <A_1 | \mu_x | \Psi^\circ(1B_2)>$$

$$\Psi^1(B_1^z;1B_2) : <B_1 | \mu_z | \Psi^\circ(1B_2)>$$

and the matrix elements listed above are between zeroth-order wavefunctions for the $\tilde{X}$ or $1B_2$ states and the manifold of states having the specified symmetry.

20

Table 4. Reference CSFs Used in CI for Cis-bending Conformations C$_{2v}$ Symmetry) and Total Number of CSFs Generated Per IRREP[a]

MO:	2a$_1$	3a$_1$	4a$_1$	5a$_1$	6a$_1$	7a$_1$	8a$_1$	1b$_1$	2b$_1$	2b$_2$	3b$_2$	4b$_2$	1a$_2$	2a$_2$
IRREP														
A$_1$ (272812)[b]	2	2	2	-	-	-	-	2	-	2	-	-	-	-
	2	2	-	-	-	-	-	2	-	2	-	2	-	-
	2	2	1	-	-	-	-	1	-	2	-	1	1	-
	2	2	2	1	-	-	-	-	-	2	-	-	2	-
	2	2	1	-	-	-	-	2	-	2	-	-	-	-
	2	2	1	-	-	-	-	2	-	2	-	-	-	-
	2	2	1	-	1	1	-	2	-	2	-	-	-	-
	2	2	1	-	1	-	-	-	-	2	-	-	2	-
A$_2$ (186990)	2	2	1	-	-	-	-	2	-	2	-	-	1	-
	2	2	2	-	-	-	-	1	-	2	-	1	-	-
	2	2	2	-	-	-	-	1	-	2	1	-	-	-
	2	2	1	-	-	-	-	2	-	2	-	-	-	-
	2	2	-	-	-	-	-	1	-	2	1	2	-	-
B$_1$ 217984	2	2	2	1	-	-	-	1	-	2	-	-	-	-
	2	2	2	-	2	-	-	1	-	2	-	-	-	-
	2	2	2	1	-	1	-	1	-	2	-	-	-	-
	2	2	-	-	1	-	-	1	-	2	-	2	-	-
	2	2	-	-	-	-	-	1	-	2	-	2	-	-
	2	2	2	-	-	-	1	1	-	2	-	-	-	-
B$_2$ (150241)	2	2	1	-	-	-	-	2	-	2	-	1	-	-
	2	2	2	-	-	-	-	1	-	2	-	-	1	-
	2	2	1	-	-	-	-	2	-	2	1	-	-	-
	2	2	1	-	-	-	-	-	-	2	1	-	2	2

[a] The 1a$_1$ and 1b$_2$ MOs, which correspond to the carbon inner shells, were treated as frozen core orbitals in the CI.
[b] Total CSFs per IRREP.

21

3.2.3 $\bar{\mathcal{B}}_o$ Over Perturbed Wavefunctions.

Expanding the cross products and dot products in Equation 3 and inserting the definitions for the perturbed wavefunctions from Equations 30 gives $\bar{\mathcal{B}}_o^\dagger$

$$\bar{B}_o^\dagger = \frac{2Im}{3}\left[\left\{<\Psi^o(\tilde{X})\,|\,m_y\,|\,\Psi^o(1B_2)><\Psi^o(1B_2)\,|\,m_z\,|\,\Psi^1(B_2^x;\tilde{X})>\right.\right.$$

$$-<\Psi^o(\tilde{X})\,|\,m_y\,|\,\Psi^o(1B_2)><\Psi^o(1B_2)\,|\,m_x\,|\,\Psi^1(A_2^z;\tilde{X})>\Big\}$$

$$-\Big\{<\Psi^o(\tilde{X})\,|\,m_y\,|\,\Psi^o(1B_2)><\Psi^o(\tilde{X})\,|\,m_z\,|\,\Psi^1(A_1^x;1B_2)>$$

$$\left.\left.-<\Psi^o(\tilde{X})\,|\,m_y\,|\,\Psi^o(1B_2)><\Psi^o(\tilde{X})\,|\,m_x\,|\,\Psi^1(B_1^z;1B_2)>\right\}\right]. \tag{31}$$

Finally, for each matrix element in Equation 31, we obtain the vibrationally-averaged electric transition dipole moments as described above.

Using the nomenclature established for the $\tilde{B}\leftarrow\tilde{X}$ transition, the final form for $\bar{\mathcal{B}}_o$, which includes vibrational averaging, is

$$\bar{B}_o = \frac{2Im}{3}\left[\left\{S(\tilde{X}\,|\,1B_2)_{v'v''}^y \cdot S(1B_2\,|\,(B_2^x;\tilde{X}))_{v'v''}^z - S(\tilde{X}\,|\,1B_2)_{v'v''}^y \cdot S(1B_2\,|\,(A_2^z;\tilde{X}))_{v'v''}^x\right\}\right.$$

$$\left.-\left\{S(\tilde{X}\,|\,1B_2)_{v'v''}^y \cdot S(\tilde{X})\,|\,(A_1^x;1B_2))_{v'v''}^z - S(\tilde{X}\,|\,1B_2)_{v'v''}^y \cdot S(\tilde{X}\,|\,(B_1^z;1B_2))_{v'v''}^x\right\}\right]. \tag{32}$$

4. RESULTS AND DISCUSSION

4.1 $\tilde{B}\leftarrow\tilde{X}$ Transition; Trans-bending.

Figure 2 shows the electric dipole transition moments between the zeroth-order states including $<\tilde{X}\,|\,m_x\,|\,\tilde{B}>$, $<\tilde{X}\,|\,m_y\,|\,\tilde{B}>$, and $<\tilde{X}\,|\,m_z\,|\,2A_u>$ as a function of bend angle. The actual values are listed in Table 5. The magnitudes of the moments are essentially zero at 180° and increase with bend angle. The $<\tilde{X}\,|\,m_y\,|\,\tilde{B}>$ shows a maximum near 140°, which coincides with the equilibrium bend angle in $\tilde{B}$ using the ground state bond lengths. Our $<\tilde{X}\,|\,m_x\,|\,2A_u>$ curve is not as smoothly varying as the other two moments in Figure 2 due to an avoided crossing of the 2A_u and 3A_u states in the region of 130-140°. Also, the fact that $<\tilde{X}\,|\,m_x\,|\,\tilde{B}>$
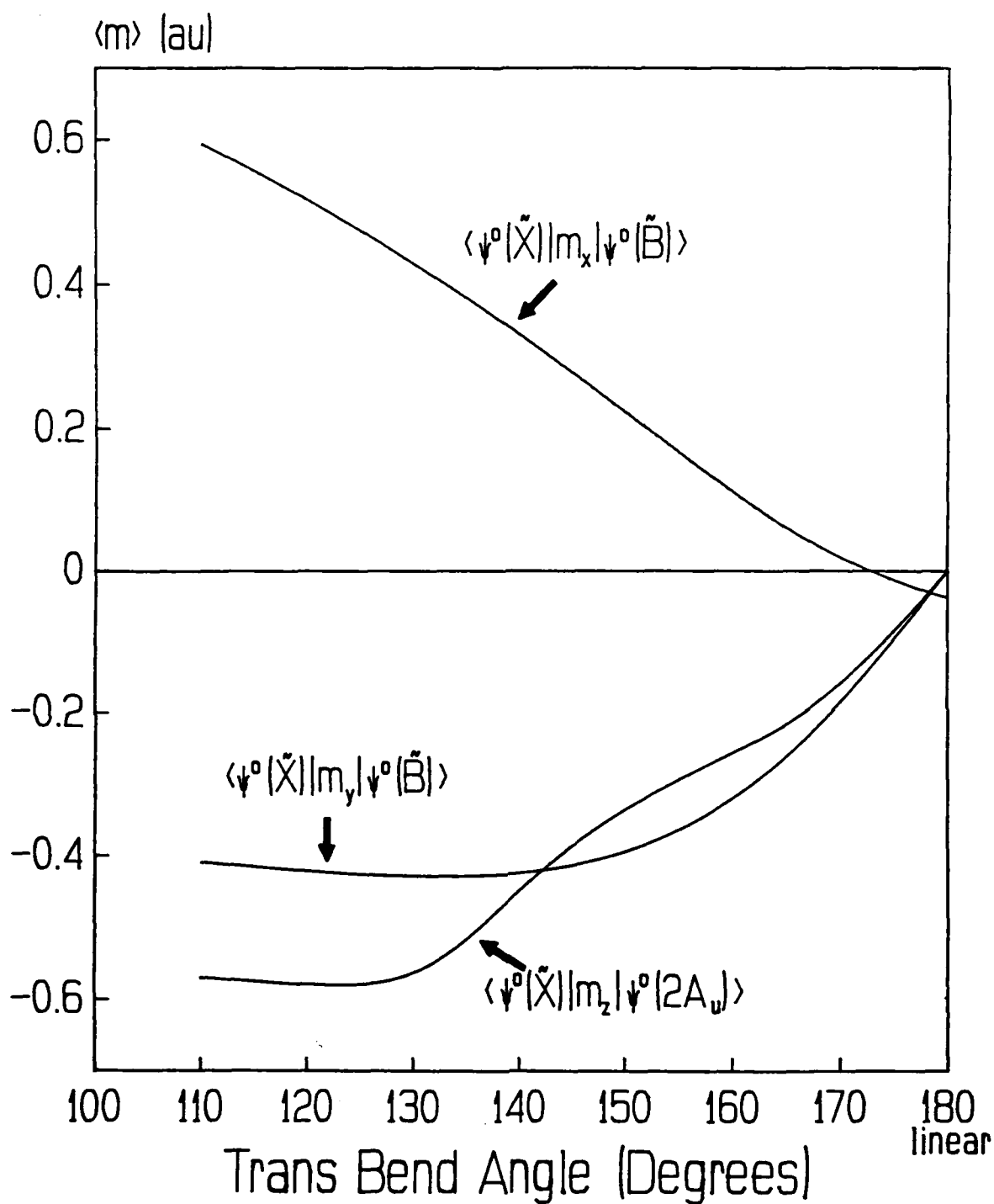
Figure 2. Electric Dipole Transition Moments Between the Ground State and the Components of the $1^1\Delta_u(2^1A_u, 1^1B_2$ as a Function of Trans-bend Angle. All Moments are Over Zeroth-Order Wavefunctions.

23

Table 5. The Electric Dipole Transition Moments (in au) vs. the Trans-bending Angle for Matrix Elements Involving the Zeroth-Order Wavefunctions for the $\tilde{X}$, $\tilde{B}$, and $2A_u$ States

Angle (Deg)	$<\tilde{X}\,\|\,m_x\,\|\,\tilde{B}>$	$<\tilde{X}\,\|\,m_y\,\|\,\tilde{B}>$	$<\tilde{X}\,\|\,m_z\,\|\,2A_u>$
180 (linear)	-0.0394	0.	0.
170	0.0066	-0.1995	-0.1800
160	0.1071	-0.3312	-0.2564
150	0.2224	-0.4009	-0.3283
140	0.3321	-0.4276	-0.4398
130	0.4294	-0.4297	-0.6003
120	0.5189	-0.4213	-0.5790
110	0.5929	-0.4077	-0.5686

is small but non-zero at 180° is an artifact of the calculations induced by a minor symmetry breaking in the wavefunction at 180°. Its effect on the final transition intensities was tested by setting the moment to zero at 180° and rerunning the vibrational analysis. The final MCD intensities for the 0-0 and 0-1 transitions changed by $\leq 0.5\%$, which is quite acceptable for this study.

PPB have also calculated these moments. The agreement between the present result and that of PPB is quite good for the $<\tilde{X}\|m_y\|\tilde{B}>$ curve, with both showing a maximum near 140°. Their $<\tilde{X}\|m_x\|\tilde{B}>$ and $<\tilde{X}\|m_z\|2A_u>$ moments show the same qualitative dependence on bend angle as what is found here. However, there are quantitative discrepancies between the studies ranging from a few percent to approximately 20%, with the larger difference occurring for $<\tilde{X}\|m_x\|\tilde{B}>$ at angles less than 130°. Given the differences in approach between the two studies, including their use of a smaller AO basis set, different bond lengths, and a different CI approach, it would be very difficult, if not impossible (and outside the purpose of this study), to unambiguously determine the source of these discrepancies in the moments.

4.1.1 Oscillator Strengths. The absorption oscillator strengths for the $\tilde{B}\leftarrow\tilde{X}$ transition have been calculated and are given in Table 6. The 1-0 band carries the largest oscillator strength of $f_{abs}=0.0025$. This can be compared to the experimental spectrum of Foo and Innes (1973) which has the intensity peaking around v'=3-5. It is difficult to make any further comparison with experiment due to the complicated, diffuse nature of the spectrum, and the absence of an experimental estimate for the oscillator strength.

Table 6. Calculated Absorption Oscillator Strengths for the $\tilde{B}\leftarrow\tilde{X}$ Transition Resulting From the Vibrational Analysis on the Trans-bending Mode

v'-v"	$f_{abs}\times10^3$
0-0	0.905
1-0	2.490
2-0	0.478
3-0	0.281
4-0	0.301
5-0	0.146

4.1.2 MCD Intensities. Equation 14 shows the transition moments needed to calculate the MCD for the trans-bending mode. There are two main parts to Equation 14. The first part, labeled 14a, accounts for the perturbation of the ground state and the second part, labeled 14b, describes the perturbation of the excited $\tilde{B}$ state. Due to the rather large energy separation of the ground state from the nearest excited gerade state (i.e., $1\Pi_g$: $T_e \geq 8.59$eV from these calculations), one would expect the first-order corrections to $\tilde{X}$ to be considerably smaller than the corrections to $\tilde{B}$; hence, Equation 14a should contribute significantly less to the MCD intensity than Equation 14b. In fact, Segal and co-workers (Dutch and Segal 1983; Diamond and Segal 1984) have shown this to be true in other cases, thus often enabling one to ignore the first term in Equation 14 at a considerable computational saving.

Figure 3 shows the angle dependence of the orbital angular momentum matrix elements between the quasi-degenerate states $\tilde{B}$ and $2A_u$($<\Psi^\circ(2A_u)|L_x|\Psi^\circ(\tilde{B})>$ and $<\Psi^\circ(2A_u)|L_y|\Psi^\circ(\tilde{B})>$) over their zeroth-order wavefunctions. For a $^1\Delta$ state (linear geometry), the matrix element $<\Psi^\circ(2A_u)|L_x|\Psi^\circ(\tilde{B})>$ should be 2 and $<\Psi^\circ(2A_u)|L_y|\Psi^\circ(\tilde{B})>$ should be 0, consistent with the results in Figure 3. The $<\Psi^\circ(2A_u)|L_x|\Psi^\circ(\tilde{B})>$ value drops to 1.06 au at 90° while the $<\Psi^\circ(2A_u)|L_y|\Psi^\circ(\tilde{B})>$ increases to 0.75 au. These matrix elements are necessary for determining the perturbation of $\tilde{B}$ by its quasi-degenerate partner $2A_u$. Equations 16 and 29 show the contribution of the $2A_u$-$\tilde{B}$ interaction to the MCD (with v'=K) to be proportional to

$$< \chi^x_{v''}(R) \mid < \Psi^\circ(\tilde{X}) \mid m_y \mid \Psi^\circ(\tilde{B})> \mid \chi^x_{v'}(R)><\chi^x_{v''}(R) \mid < \Psi^\circ(\tilde{X}) \mid m_z \mid \Psi^\circ(2A_u)> \mid \sum_\lambda d^K_{2A_u^x\lambda}\chi^{2A_u}_\lambda(R)>.$$

$\langle L \rangle$ (au)

$\langle \psi^{\circ}(2A_u)|L_x|\psi^{\circ}(\widetilde{B})\rangle$

$\langle \psi^{\circ}(2A_u)|L_y|\psi^{\circ}(\widetilde{B})\rangle$

Trans Bend Angle (Degrees)
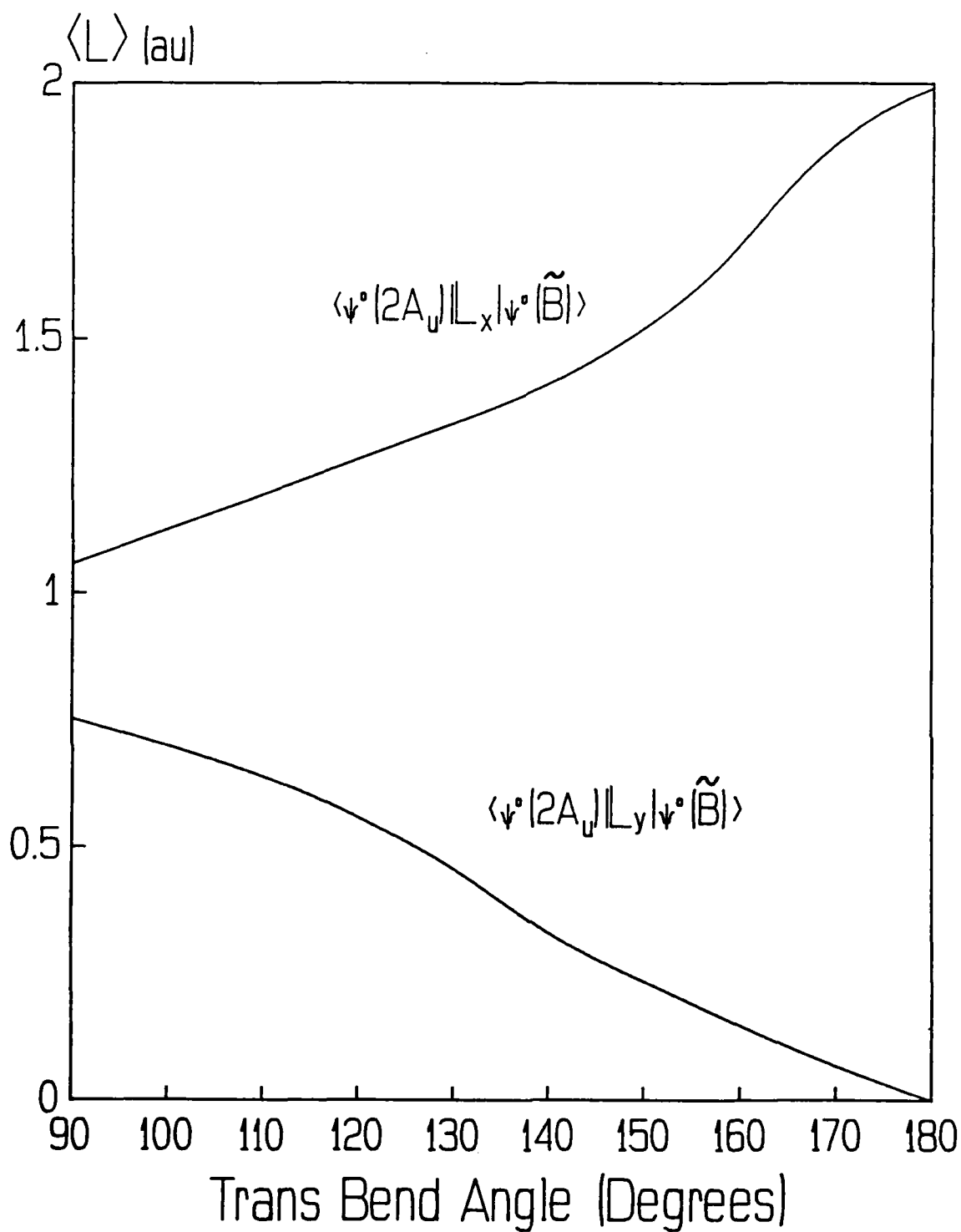
Figure 3. Orbital Angular Momentum Matrix Elements $\langle \vec{L} \rangle$ Coupling the Zeroth-Order Wavefunctions for the 2^1A_u and 1^1B^u Components of the $1^1\Delta^u$. The Moments are Plotted as a Function of Trans-bend Angle (All Values are in Atomic Units). The Magnetic Dipole Moments $\langle \vec{m} \rangle$ are Related (in au) to Orbital Angular Momentum by $\langle \vec{m} \rangle = (1/2)\langle \vec{L} \rangle$.

26

The PES for the $2A_u$ requires some discussion. Peric, Peyerimhoff, and Buenker found in their calculations that the $2A_u$ state prefers a non-planar structure with a twist of approximately 90° about the C-C for non-linear conformations. It is beyond the scope of this study to attempt a multi-dimensional vibrational treatment, therefore the molecule is assumed to remain planar in the $2A_u$ state. This limits our ability to calculate an accurate vibronic coupling between the $\tilde{B}$ and $2A_u$, since quasi-degenerate perturbation theory requires PESs for both states. In analyzing the make-up of the vibronic wavefunction, Ψ_K, one finds the encouraging result that the largest contribution to the first two vibronic states, $\Psi_K(v_K=0,1)$, come almost entirely from couplings with the $v=0,1$ of the $2A_u$. So it is reasonable to expect the Ψ_K's to be good approximations to the true wavefunctions for $v_K=0,1$, and the calculations to predict MCD intensities for the 0-0 and 1-0 bands in reasonable agreement with experiment.

Figure 4 shows the plots of the electric dipole transition moment matrix elements between the zeroth-order excited $\tilde{B}$ state and the first-order correction to the ground state, $\Psi^1(B_g;\tilde{X})$. These matrix elements are found in Equation 14a. Figure 5 plots matrix elements between the zeroth-order ground state wavefunction and the first-order correction to the $\tilde{B}$ state (Equation 14b). It is immediately clear from comparing Figures 4 and 5 that the absolute magnitudes of the moments involving the perturbed excited $\tilde{B}$ state are considerably larger than those of the perturbed $\tilde{X}$ state over most of the PES.

By inspection of Figure 5, one sees that the largest matrix element in the vicinity of the equilibrium bend angle for the $\tilde{B}$ state is $<\Psi^o(\tilde{X})\,|\,m_z\,|\,\Psi^1_Q(A_u^x;\tilde{B})>$, which represents the coupling of $\tilde{B}$ with the A_u states over μ_x. This matrix element does not include the contribution from $\tilde{B}$ coupling to its quasi-degenerate partner, the $2A_u$. It is left to the vibrational treatment to account for this $\tilde{B}$-$2A_u$ interaction. The results of the vibrational treatment are given in Table 7, which lists the contributions from each matrix element in Equation 14 to each vibrational band. The matrix elements $<\Psi^o(\tilde{X})\,|\,m_z\,|\,\Psi^1(A_u^x;\tilde{B})>$ and $<\Psi^o(\tilde{X})\,|\,m_z\,|\,\Psi^1(A_u^y;\tilde{B})>$ now contain both the non-degenerate and quasi-degenerate (i.e., $\tilde{B}$-$2A_u$) PT contributions. It can be seen that the matrix element involving $\Psi^1(A_u^x;\tilde{B})$ is by far the single largest contributor to the intensity for the two vibrational bands. Specifically, the $\tilde{B}\leftarrow\tilde{X}$ transition gains much of its MCD intensity through interactions with A_u states. As in absorption, the more intense MCD band is the 1-0. The calculated $\Delta\varepsilon_o^{max}s$ are (0-0)=-3.48, (1-0)=-5.82. Table 7 also lists (in parenthesis) the corresponding experimental $\Delta\varepsilon_o^{max}$ values; (0-0)≈-0.8, (1-0)≈-1.6. The theoretical values for (0-0) and (1-0) are a factor of 4 larger than the
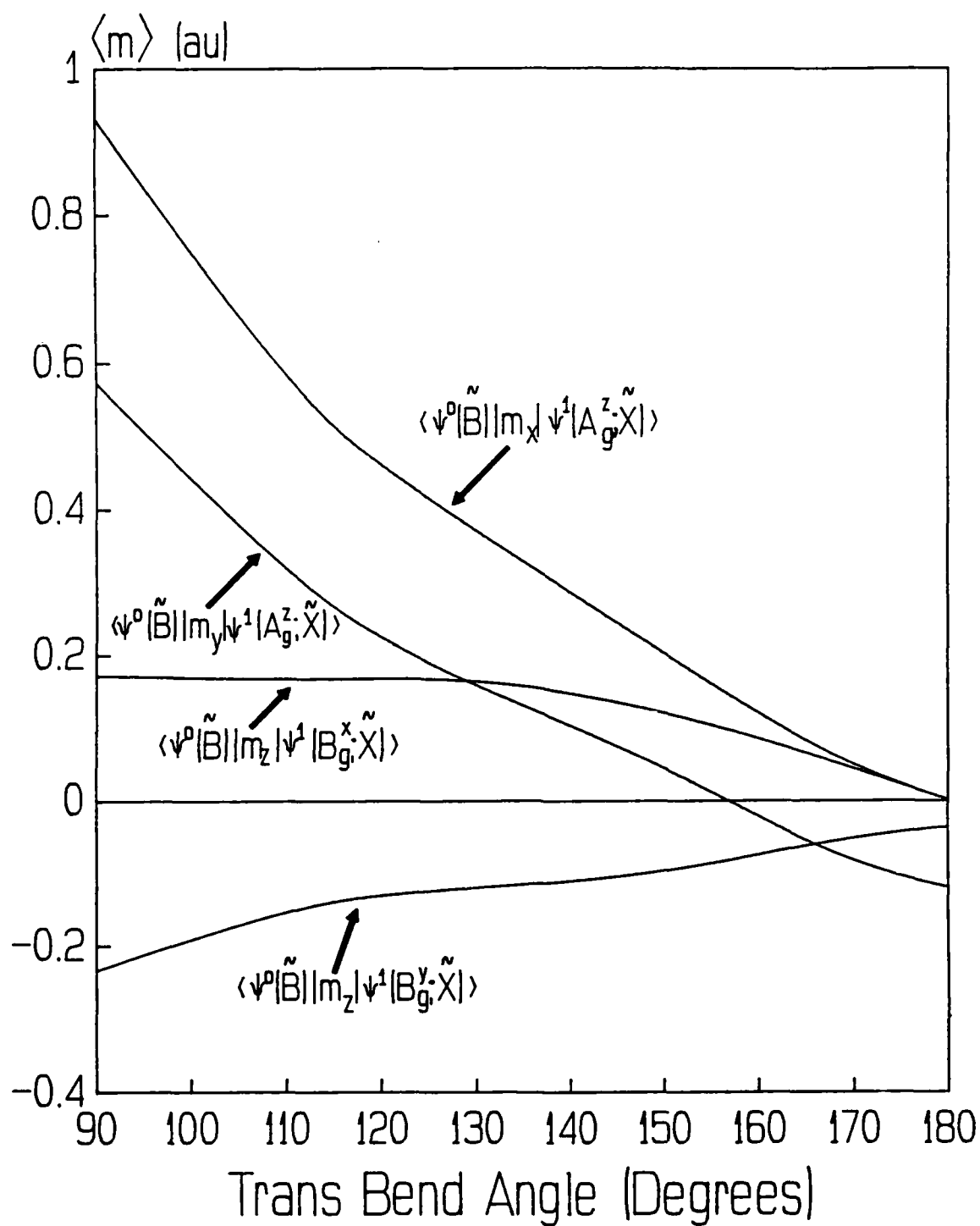
Figure 4. Electric Dipole Transition Moments as a Function of Trans-bend Angle. The Matrix Elements Include the First-Order Correction to the Wavefunction for the Perturbed Ground State. All Values are in Atomic Units. See Equation 13 for Definitions of First-Order Wavefunctions.
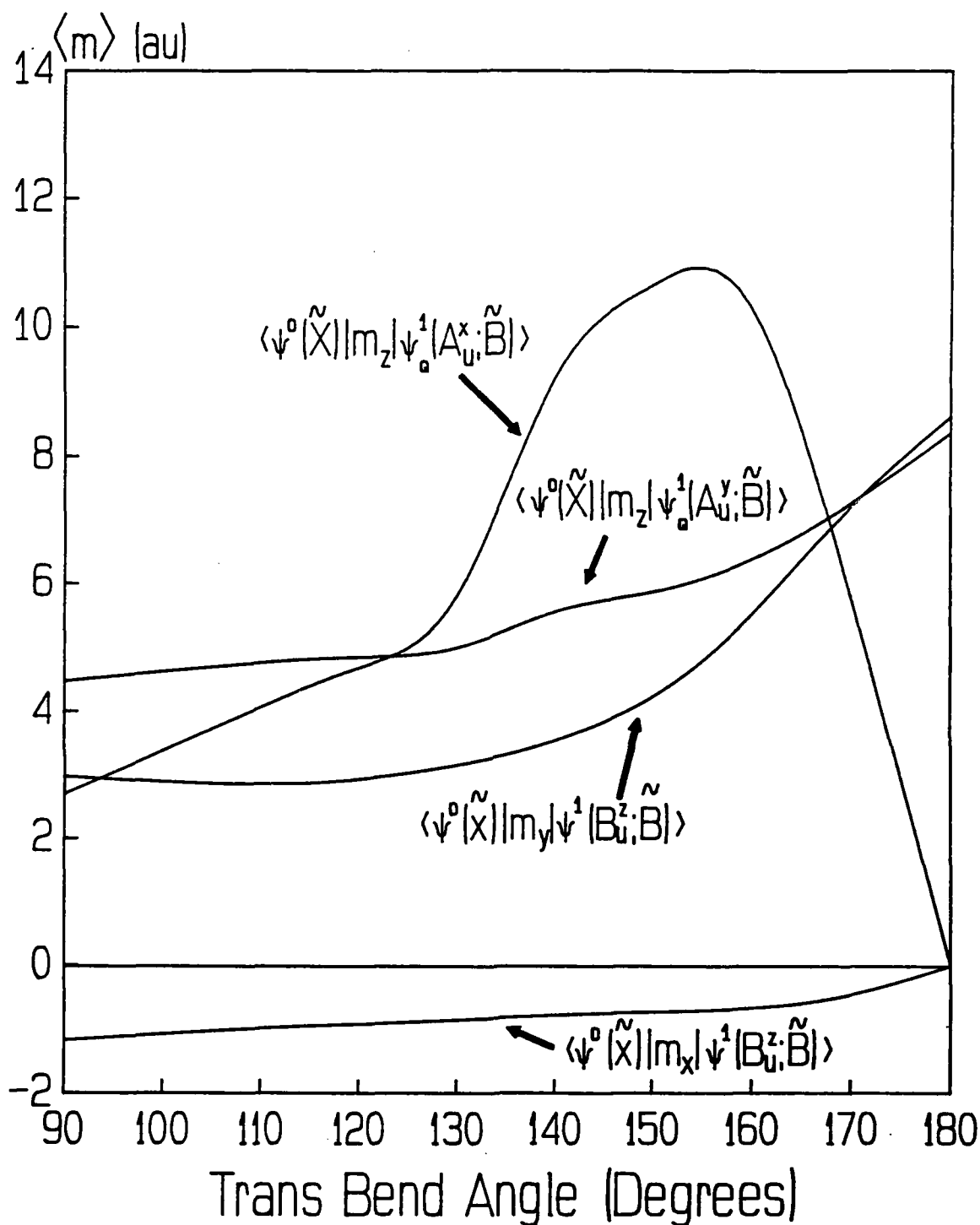
Figure 5. Electric Dipole Transition Moments as a Function of Trans-bend Angle for $\tilde{B}\leftarrow\tilde{X}$. The Matrix Elements Include the Total First-Order Correction to the Wavefunction for the Perturbed $\tilde{B}$ State. All Values are in Atomic Units. See Equation 13 for Definitions of First-Order Wavefunctions.

Table 7. Electric Dipole Transition Moment Components (in au) Determining the MCD Intensity for the $\tilde{B}\leftarrow\tilde{X}$ Transition (Trans-bending Motion)

	v'-v"		
	0-0	1-0	
$<\Psi^o(\tilde{X})\|m_x\|\Psi^o(\tilde{B})>$	-.0201149	+.0105815	Zeroth-order
$<\Psi^o(\tilde{X})\|m_y\|\Psi^o(\tilde{B})>$	+.0696649	-.1190800	Moments
$<\Psi^o(\tilde{B})\|m_z\|\Psi^1(B_g^x;\tilde{X})>$	-.0180523	+.0280062	
$<\Psi^o(\tilde{B})\|m_z\|\Psi^1(B_g^y;\tilde{X})>$	+.0175951	-.0354671	Perturbing the
$<\Psi^o(\tilde{B})\|m_y\|\Psi^1(A_g^z;\tilde{X})>$	+.0114457	-.0566385	$\tilde{X}$ state
$<\Psi^o(\tilde{B})\|m_x\|\Psi^1(A_g^z;\tilde{X})>$	-.0246575	+0.3196930	
$<\Psi^o(\tilde{X})\|m_z\|\Psi^1(A_u^x;\tilde{B})>$	+16.3245000	-19.7214400	
$<\Psi^o(\tilde{X})\|m_z\|\Psi^1(A_u^y;\tilde{B})>$	-.8072640	-2.7946300	Perturbing the
$<\Psi^o(\tilde{X})\|m_y\|\Psi^1(B_u^z;\tilde{B})>$	-1.6048100	-4.9070150	$\tilde{B}$ state
$<\Psi^o(\tilde{X})\|m_x\|\Psi^1(B_u^z;\tilde{B})>$	+.1523540	+.2918810	
$\tilde{\mathcal{B}}_0$[a]	-.224x10^{-4}	-.463x10^{-4}	
$\Delta\varepsilon_o^{max}$[b] (cgs units)	-3.48 (-0.8)[c]	-5.82 (-1.6)	MCD Band Maxima (Experimental Maxima)

[a] Consistent with electric dipole moments in debye.
[b] Gaussian band shape described in text with $\Delta=120cm^{-1}$(0-0), $150cm^{-1}$(1-0), and $\tilde{u}_o=54116cm^{-1}$(0-0), $54794cm^{-1}$(1-0).
[c] Experimental values from Gedenken and Schnepp (1976).

experimental maxima, but of the correct sign. This agreement is acceptable considering the approximate nature of the vibrational treatment.

4.2 $\underline{1B_2\leftarrow\tilde{X}\text{ Transition; Cis-bending}}$. Theory suggests (vide supra) that the $1B_2\leftarrow\tilde{X}$ transition might overlap the $\tilde{B}\leftarrow\tilde{X}$ band system and be responsible for part of the irregular band shapes and variations in intensities. In this section, we examine the predicted MCD and absorption intensities (i.e., oscillator strengths) for the $1B_2\leftarrow\tilde{X}$ transition and compare these to the analogous values for the $\tilde{B}\leftarrow\tilde{X}$ system.

4.2.1 Oscillator Strengths. The y-component of the electric dipole transition moment for $1B_2 \leftarrow \tilde{X}$ is shown as a function of bending in Figure 6. Again, the $1B_2$ state is one of the degenerate partners in the $1\Delta_u$ state (see Figure 1); thus, the electric dipole transition moment must be zero at 180°. The curve in Figure 6 shows the moment continually increasing from essentially zero at 180° to 0.58 au at 110°, the largest angle calculated. Once again, Peric, Peyerimhoff, and Buenker have calculated this electric dipole moment and found a similar qualitative dependence on bend angle. However, the magnitude of thechange per degree is larger in PPBs study than here. For example, at an angle of 110° they predict a moment of $\approx |0.80|$ while our value is $|0.58|$. The reader is referred to the section concerning the $\tilde{B} \leftarrow \tilde{X}$ transition for a discussion of possible causes for this quantitative difference in the moments between the two studies. Table 8 lists the values of the electric dipole transition moment plotted in Figure 6.

The calculated 0-0 transition energies for the $\tilde{B} \leftarrow \tilde{X}$ and $1B_2 \leftarrow \tilde{X}$ band systems are $\Delta E = 56667 cm^{-1} (\tilde{B} \leftarrow \tilde{X})$ and $\Delta E = 56330 cm^{-1} (1B_2 \leftarrow \tilde{X})$, which do indeed lie close to one another. The calculated transition energies for excitations from v"=0 to v'=0,1,2,3 are given in Table 9 along with the experimental values for the $\tilde{B} \leftarrow \tilde{X}$ reported by Foo and Innes (1973).

Table 8. Electric Dipole Transition Moment vs. Cis-bend Angle for the Matrix Element Involving the Zeroth-order $\tilde{X}$ and $1B_2$ States

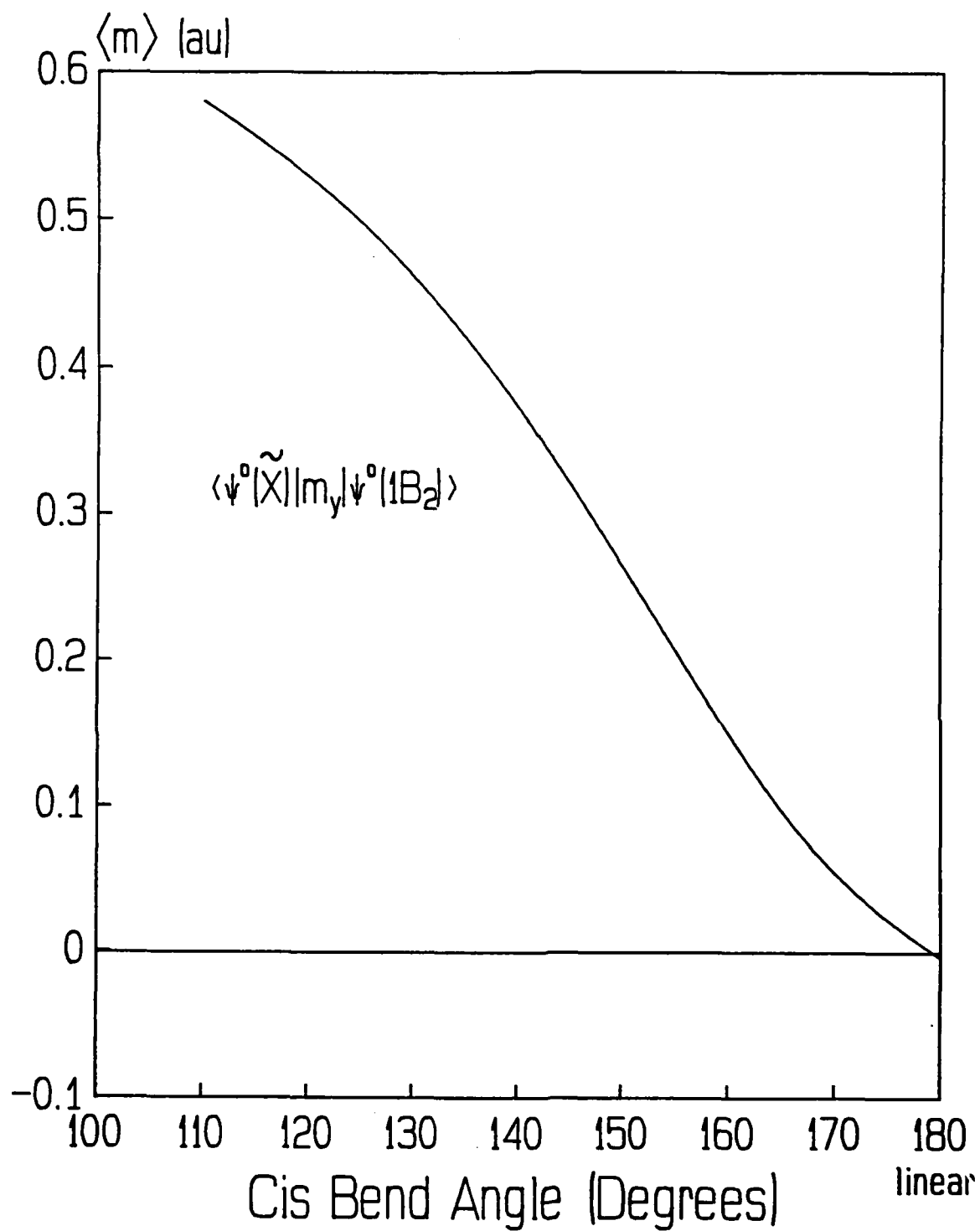| Angle (Deg)	$<\tilde{X}(1^1A_1)\,|m_y|\,1^1B_2>$
180 (linear)	-0.0036
170	0.0416
160	0.1461
150	0.2662
140	0.3760
130	0.4659
120	0.5327
110	0.5798

31

Figure 6. The Y-Component of the Electric Dipole Transition Moment as a Function of Cis-bend Angle for the $1B_2 \leftarrow \tilde{X}$ Transition Over Zeroth-Order Wavefunctions.

32

Table 9. Transition Energies (in cm^{-1}) for the $\tilde{B}\leftarrow\tilde{X}$ and $1B_2\leftarrow\tilde{X}$ Band Systems

v'-v"	$\tilde{B}\leftarrow\tilde{X}^a$	$\Delta E(v'_{i+1}-v'_1)$	$\tilde{B}\leftarrow\tilde{X}^b$	$\Delta E(v'_{i+1}-v'_1)$	$1B_2\leftarrow\tilde{X}^a$
0-0	56667.		54116.		56330.
1-0	57296.	629.	54850.	734.	56988.
2-0	57756.	460.	55538.	688.	57585.
3-0	58398.	642.	56285.	743.	58070.
4-0	59227.	829.	56984.	699.	58523.
5-0	60170.	943.	57827.	843.	59116.

[a] From PESs using minimum energy band lengths for both states. See text, Section 3.
[b] Experimental values from Foo and Innes (1973).

The oscillator strengths for absorption are given in Table 10. The transitions to the first four v' levels are shown, and one finds the 2-0 band predicted to be the most intense with $f_{abs}=4.4\times10^{-5}$, and 15 times more intense that the 0-0. The important point to note is that the magnitude of the 2-0 is approximately a factor of 60 less intense than the strongest band in the $\tilde{B}\leftarrow\tilde{X}$

Table 10. Calculated Absorption Oscillator Strengths for the $1B_2\leftarrow\tilde{X}$ Transition

v'-v"	$f_{abs}\times10^5$
0-0	0.2820
1-0	1.6800
2-0	4.3800
3-0	3.0200
4-0	0.0146

4.2.2 MCD Intensities. Unlike the $\tilde{B}$ state, the $1B_2$ has no allowed magnetic dipole coupling to its quasi-degenerate partner, the $2A_2$. This is significant because the theoretical study of Peric, Peyerimhoff, and Buenker found the $2A_2$ (like the $2A_u$) component of the $1\Delta_u$ prefers a twisted conformation at larger bend angles. The lack of magnetic dipole coupling between $1B_2$ and $2A_2$ simplifies the calculation of the MCD for the $1B_2\leftarrow\tilde{X}$ because quasi-degenerate PT is not needed. But, more importantly, this removes the uncertainty in the calculated MCD added by having to couple to a PES (i.e., the $2A_2$) which is known to be inaccurate at higher vibrational levels.

33

Table 11 gives the MCD $\Delta\varepsilon_o^{max}$ for the first six vibrational bands. The vibrational levels 4-0 and 5-0 are found to be opposite in sign to the first four bands. One important observation from Table 11 is that matrix elements involving the perturbed ground state contribute significantly to the total MCD intensity for the 0-0, 1-0, and 2-0 bands. This arises not because of large perturbation to the ground state, but because the two components describing the perturbation to the $1B_2$ state are nearly equal in magnitude and cancel one another. This is in contrast to what we saw in the $\tilde{B}\leftarrow\tilde{X}$ band system where essentially all the MCD intensity arose from perturbations of the excited state $\tilde{B}$, not the ground state. The other important observation is that the strongest band, the 3-0, has a predicted MCD intensity of $\Delta\varepsilon_o^{max} = -.0037$, which is three orders of magnitude smaller than in the $\tilde{B}\leftarrow\tilde{X}$. Part of the explanation for this relatively small MCD signal lies in the symmetry of the molecule which dictates the allowed magnetic dipole couplings and therefore the ability to borrow transition intensity. It will be informative to look at the states closest in energy to the $1\Delta_u$, since these should couple most strongly with the components of the $1\Delta_u$.

Peric, Buenker, and Peyerimhoff (1984, 1987) calculated the lowest 16 singlet states in the linear conformation, and the energies of the lowest five states are shown in Table 12, with the spread in ΔE due to different choices in reference CSFs. As a reminder, the $1\Delta_u$ splits into the $(2A_2, 1B_2)$ (cis-bending) and $(2A_u, 1B_u)$ (trans-bending). Table 12 shows its nearest neighbors to be the $1\Sigma_u^-$ and $1\Pi_u$.

It has already been demonstrated that in the trans-bending case, the $\tilde{B}$ state can borrow intensity from any A_u and B_u state. This includes its quasi-degenerate partner, the $2A_u$, and the components making up both the $1\Sigma_u^-$ (A_u) and $1\Pi_u(A_u, B_u)$ states. Since these four neighboring "states" (in C_{2h}) lie within $\approx 0.35e$ of the $\tilde{B}$ state (in the linear geometry), perturbation theory would predict potentially large borrowing of intensity from these four states by $\tilde{B}$, and hence a strong MCD signal.

If the same rationale is applied to the cis-bending mode, its C_{2v} symmetry disallows any interaction of the $1B_2$ state with any A_2 state, including its quasi-degenerate partner the $2A_2$ and its lower energy neighbor the $1\Sigma_u^-$ (A_2). Therefore, in the reduced C_{2v} symmetry, the $1B_2$ can borrow intensity from only two of its four closest neighbors which are the components of the $1\Pi_u(A_1, B_1)$. The next nearest allowed coupling is with the $1\Delta_g$, which lies $\approx 1.3eV$ (linear geometry) above the $1\Delta_u$. Peric, Buenker,

Table 11. Electric Dipole Transition Moment Components (in au) Determining the MCD Intensity for the $1B_2 \leftarrow \tilde{X}$ Transition (Cis-bending Motion)[a]

	0-0	1-0	2-0	3-0	4-0	5-0	
$\langle\Psi^\circ(\tilde{X})|m_y|\Psi^\circ(1^1B_2)\rangle$	+.004061	-.009846	+.015814	-.013087	-.000905	+.007302	Zeroth-order Moments
$\langle\Psi^\circ(1^1B_2)|m_z|\Psi^1(B_2^x;\tilde{X})\rangle$	-.016154	+.040388	-.074970	+.093381	-.047028	+.008793	Perturbing the $\tilde{X}$ State
$\langle\Psi^\circ(1^1B_2)|m_x|\Psi^1(A_2^t;\tilde{X})\rangle$	-.013435	+.035486	-.069144	+.089181	-.045825	+.007985	
$\langle\Psi^\circ(\tilde{X})|m_z|\Psi^1(A_1^x;1^1B_2)\rangle$	+.167516	-.634827	+1.81626	-3.43442	+2.80941	-1.40362	Perturbing the $1B_2$ State
$\langle\Psi^\circ(\tilde{X})|m_x|\Psi^1(B_1^t;1^1B_2)\rangle$	+.167736	-.625046	+1.77598	-3.35618	+2.75353	-1.38737	
$\bar{R}_0$[b]	$-.199\times10^{-9}$	$-.284\times10^{-8}$	$-.143\times10^{-7}$	$-.212\times10^{-7}$	$+.101\times10^{-8}$	$+.244\times10^{-8}$	MCD Band Maxima
$\Delta\varepsilon_0^{max}$[c] (cgs units)	-.0000309	-.000357	-.00218	-.00370	+.000157	+.000593	

[a] All moments in atomic units.
[b] Consistent with electric dipole moments in debye.
[c] Gaussian band shape function described in text with parameters Δ and $\bar{\nu}_0$ arbitrarily chosen to be the same as for the corresponding vibrational bands in the $\tilde{B}-\tilde{X}$ band system (Foo and Innes 1973); $\Delta=111\text{cm}^{-1}$(4-0), 127cm^{-1}(3-0), 82cm^{-1}(5-0), and $\bar{\nu}_0=56285\text{cm}^{-1}$(3-0), 56984cm^{-1}(4-0), 57827cm^{-1}(5-0), and see footnotes in Table 7.

Table 12. Vertical Excitation Energies for Linear Acetylene[a]

State $(D_{\infty h})$	$\Delta E(eV)$
$1\Pi_g$	8.38-8.46
$1\Pi_u$	7.92-8.00
$1\Delta_u$	7.56-7.65
$1\Sigma_u^-$	7.21-7.32
$1\Sigma_g^+$	0

[a] From ab initio MRD-CI calculations (Peric, Buenker, and
Peyerimhoff 1984).

and Peyerimhoff (1984, 1987) also reported the cis- and trans-PESs associated with the 16 lowest singlet $D_{\infty h}$ states, and these curves clearly show the ΔE between the $1B_2$ and all higher lying states increases rapidly with bend angle. In fact, their curves predict that this increase is more pronounced for the $1B_2$ than for $\tilde{B}$, again suggesting less ability for the $1B_2$ to borrow intensity from neighboring states than what we see for the $\tilde{B}$ state.

Therefore, both perturbative (i.e., based on energetics) and symmetry arguments can be used to explain the calculated results which show the MCD intensity to be significantly weaker in the $1B_2 \leftarrow \tilde{X}$ transition than in the $\tilde{B} \leftarrow \tilde{X}$

5. CONCLUSIONS

A new method has been presented for predicting *a priori* the MCD spectrum in molecules. The method, based on first-order perturbation theory, significantly reduces the time consuming process of explicitly calculating a large number of excited electronic states which might be needed to satisfy the summation in the first-order perturbation expression in Equation 9. As an initial test case, this method has been used here to study the character of the experimental MCD spectrum associated with the $\tilde{B} \leftarrow \tilde{X}$ electronic transition in acetylene. The MCD and absorption intensities for the $1B_2 \leftarrow \tilde{X}$ transition were also determined to assess the possibility that the irregularities seen in the 185-170 nm spectral region result from the $1B_2 \leftarrow \tilde{X}$ band system overlapping the $\tilde{B} \leftarrow \tilde{X}$

For the $\tilde{B} \leftarrow \tilde{X}$ band system, this study predicts a $\Delta\varepsilon_o^{max}$ of -3.5 and -5.8 for the 0-0 and 1-0 vibrational bands, respectively. These results agree with experiment with respect to the signs of the bands. They are also consistent with the experimentally observed trend of the $\Delta\varepsilon_o^{max}$ increasing as v' increases. However, the magnitudes are a factor of 4 larger than the experimental values of -0.8 and -1.6, respectively. This agreement is quite acceptable considering the approximations made in the vibrational treatment.

Concerning the possible overlap of the $1B_2 \leftarrow \tilde{X}$ and $\tilde{B} \leftarrow \tilde{X}$ band systems, the current study predicts the 0-0 transition energies for the two systems to lie in the same spectral region. The calculated 0-0 transition energies are $\Delta E = 56330 cm^{-1}(1B_2 \leftarrow \tilde{X})$ and $\Delta E - 56667 cm^{-1}(\tilde{B} \leftarrow \tilde{X})$. The most intense MCD band in the $1B_2 \leftarrow \tilde{X}$ band system is the 3-0 with a calculated $\Delta\varepsilon_0^{max} = -.0037$. For the $\tilde{B} \leftarrow \tilde{X}$ band system, the more intense vibrational band is predicted to have a value of $\Delta_0^{max}(1-0) = -5.82$, which is $\approx 10^3$ times larger than the $\Delta\varepsilon_0^{max}$ values calculated for the $1B_2 \leftarrow \tilde{X}$ MCD spectrum. In spite of the possibility that improvements in the theoretical treatment, especially the vibrational treatment, might cause significant changes in the calculated intensities, it seems unlikely that the MCD intensities for the $1B_2 \leftarrow \tilde{X}$ and $\tilde{B} \leftarrow \tilde{X}$ would change three orders of magnitude relative to one another. Hence, this study predicts that the irregularities in the 185-170 nm region of the MCD are not due to the overlapping of the $1B_2 \leftarrow \tilde{X}$ and $\tilde{B} \leftarrow \tilde{X}$ band systems.

With regards to the absorption intensity, the current study predicts that the oscillator strengths for the $1B_2 \leftarrow \tilde{X}$ transition are a factor of 60 smaller than those calculated for the $\tilde{B} \leftarrow \tilde{X}$, suggesting that the $1B_2 \leftarrow \tilde{X}$ would at most appear as small perturbations in the absorption spectrum of $\tilde{B} \leftarrow \tilde{X}$. One interference in the $\tilde{B} \leftarrow \tilde{X}$ absorption spectra has already been established by Foo and Innes (1973) who identified high-lying, trans-bending vibrational levels of the $\tilde{A}(1A_u) \leftarrow \tilde{X}$ transition spilling over into the $\tilde{B} \leftarrow \tilde{X}$, with the $\tilde{A} \leftarrow \tilde{X}(13-0)$ occurring at an energy slightly above the 0-0 for $\tilde{B} \leftarrow \tilde{X}$. Another possible candidate is the $2A_u \leftarrow \tilde{X}$, which is found here and by previous theory (Peric, Buenker, and Peyerimhoff 1987) to be strongly electric dipole allowed at larger bend angles and a planar conformation. However, at these bend angles, the molecule was found to prefer a twisted conformation, leading one to expect a poor Franck-Condon overlap with the ground state; and thus, predicting a potentially weak transition (Peric, Buenker, and Peyerimhoff 1987). And finally, as Peric, Peyerimhoff, and Buenker had mentioned, there are most likely strong vibrational couplings of the $2B_u$ state with other states. In

light of the results from this study and previous work by others, these couplings, along with the $\tilde{A} \leftarrow \tilde{X}$ band system, seem to be the most plausible explanations for the diffuse bands and complicated structure in the absorption spectrum of the $\tilde{B} \leftarrow \tilde{X}$ band system.

In summary, this study predicts that the $1B_2 \leftarrow \tilde{X}$ and $\tilde{B} \leftarrow \tilde{X}$ electronic transitions should occur in the same spectral region. However, these calculations do not support the hypothesis that the $1B_2 \leftarrow \tilde{X}$ band system makes a significant contribution to either the absorption or the MCD spectrum in the 185-170 nm region.

6. REFERENCES

Chabalowski, C. F., J. O. Jensen, D. R. Yarkony, and B. H. Lengsfield III. J. Chem. Phys., vol. 90, p. 2504, 1989.

Dance, D. F., and I. C. Walker. Chem. Phys Letter, vol. 18, p. 601, 1973.

Diamond, J., and G. A. Segal. J. Am. Chem. Soc., vol. 106, p. 952, 1984.

Dutch, W., and G. A. Segal. J. Chem. Phys., vol. 79, p. 2951, 1983.

Foo, P. D., and K. K. Innes. Chem. Phys. Letter, vol. 22, p. 439, 1973.

Gedanken, A., and O. Schnepp. Chem. Phys Letter, vol. 37, p. 373, 1976.

Havriliak, S. J., and D. R. Yarkony. J. Chem Phys., vol. 83, p. 1168, 1985.

Herzberg, G. Molecular Spectra and Molecular Structure: III. Electronic Spectra and Electronic Structure of Polyatomic Molecules. New York: Van Nostrand-Rheinhold, 1966.

Ingold, C. K., and G. W. King. J. Chem. Soc., pp. 2702, 1953.

Jensen, J. O., G. F. Adams, and C. F. Chabalowski. Chem. Phys. Letter, vol. 172, p. 379, 1990.

Kammer, W. E. Chem. Phys. Letter, vol. 6, p. 529, 1970.

Kammer, W. E. Chem. Phys., p. 408, 1974.

King, G. W., and C. K. Ingold. Nature, vol. 169, p. 1101, 1952.

Lassettre, E. N., A. Skerbele, M. A. Dillon, and K. J. Ross. J. Chem. Phys., vol. 48, p. 5066, 1968.

Lischka, H., and A. Karpfen. Chem. Phys., vol. 102, p. 77, 1986.

Peric, M., S. D. Peyerimhoff, and R. J. Buenker. Molec. Phys., vol. 55, p. 1129, 1985.

Peric, M., S. D. Peyerimhoff, and R. J. Buenker. Molec. Phys., vol. 62, p. 1339, 1987.

Peric, M., R. J. Buenker, and S. D. Peyerimhoff. Molec. Phys., vol. 53, p. 1177, 1984.

Piepho, S. B., and P. N. Schatz. Group Theory In Spectroscopy with Applications to Magnetic Circular Dichroism. New York: Wiley-Interscience, 1983.

Pople, J. A., R. Krishnan, H. B. Schlegel, and J. S. Binkley. Int. J. Quantum Chem., vol. 13, p. 225, 1979.

So, S. P., R. W. Wetmore, and H. F. Schaefer III. J. Chem. Phys., vol. 73, p. 5706, 1980.

Stephens, P. J. _Adv. in Chem Phys._, vol. 35, p. 197, 1976, and reference therein.

Yarkony, D. R. _J. Chem. Phys._ 89, 7324, 1988.

No of Copies	Organization	No of Copies	Organization
2	Administrator Defense Technical Info Center ATTN: DTIC-DDA Cameron Station Alexandria, VA 22304-6145	1	Commander US Army Missile Command ATTN: AMSMI-RD-CS-R (DOC) Redstone Arsenal, AL 35898-5010
1	HQDA (SARD-TR) WASH DC 20310-0001	1	Commander US Army Tank-Automotive Command ATTN: AMSTA-TSL (Technical Library) Warren, MI 48397-5000
1	Commander US Army Materiel Command ATTN: AMCDRA-ST 5001 Eisenhower Avenue Alexandria, VA 22333-0001	1	Director US Army TRADOC Analysis Command ATTN: ATRC-WSR White Sands Missile Range, NM 88002-5502
1	Commander US Army Laboratory Command ATTN: AMSLC-DL Adelphi, MD 20783-1145	(Class. only) 1	Commandant US Army Infantry School ATTN: ATSH-CD (Security Mgr.) Fort Benning, GA 31905-5660
2	Commander US Army, ARDEC ATTN: SMCAR-IMI-I Picatinny Arsenal, NJ 07806-5000	(Unclass. only) 1	Commandant US Army Infantry School ATTN: ATSH-CD-CSO-OR Fort Benning, GA 31905-5660
2	Commander US Army, ARDEC ATTN: SMCAR-TDC Picatinny Arsenal, NJ 07806-5000	1	Air Force Armament Laboratory ATTN: AFATL/DLODL Eglin AFB, FL 32542-5000
1	Director Benet Weapons Laboratory US Army, ARDEC ATTN: SMCAR-CCB-TL Watervliet, NY 12189-4050		**Aberdeen Proving Ground**
		2	Dir, USAMSAA ATTN: AMXSY-D AMXSY-MP, H. Cohen
1	Commander US Army Armament, Munitions and Chemical Command ATTN: SMCAR-ESP-L Rock Island, IL 61299-5000	1	Cdr, USATECOM ATTN: AMSTE-TD
		3	Cdr, CRDEC, AMCCOM ATTN: SMCCR-RSP-A SMCCR-MU SMCCR-MSI
1	Director US Army Aviation Research and Technology Activity ATTN: SAVRT-R (Library) M/S 219-3 Ames Research Center Moffett Field, CA 94035-1000	1	Dir, VLAMO ATTN: AMSLC-VL-D

No. of Copies	Organization	No. of Copies	Organization
4	Commander US Army Research Office ATTN: R. Ghirardelli D. Mann R. Singleton R. Shaw P.O. Box 12211 Research Triangle Park, NC 27709-2211	1	Commanding Officer Naval Underwater Systems Center Weapons Department ATTN: R. S. Lazar/Code 36301 Newport, RI 02840
2	Commander US Army, ARDEC ATTN: SMCAR-AEE-B, D. S. Downs SMCAR-AEE, J. A. Lannon Picatinny Arsenal, NJ 07806-5000	2	Commander Naval Weapons Center ATTN: T. Boggs, Code 388 T. Parr, Code 3895 China Lake, CA 93555-6001
1	Commander US Army, ARDEC ATTN: SMCAR-AEE-BR, L. Harris Picatinny Arsenal, NJ 07806-5000	1	Superintendent Naval Postgraduate School Dept. of Aeronautics ATTN: D. W. Netzer Monterey, CA 93940
1	Office of Naval Research Department of the Navy ATTN: R. S. Miller, Code 432 800 N. Quincy Street Arlington, VA 22217	3	AL/LSCF ATTN: R. Corley R. Geisler J. Levine Edwards AFB, CA 93523-5000
1	Commander Naval Air Systems Command ATTN: J. Ramnarace, AIR-54111C Washington, DC 20360	1	AL/MKPB ATTN: B. Goshgarian Edwards AFB, CA 93523-5000
1	Commander Naval Surface Warfare Center ATTN: J. L. East, Jr., G-23 Dahlgren, VA 22448-5000	1	AFOSR ATTN: J. M. Tishkoff Bolling Air Force Base Washington, DC 20332
2	Commander Naval Surface Warfare Center ATTN: R. Bernecker, R-13 G. B. Wilmot, R-16 Silver Spring, MD 20903-5000	1	OSD/SDIO/IST ATTN: L. Caveny Pentagon Washington, DC 20301-7100
5	Commander Naval Research Laboratory ATTN: M. C. Lin J. McDonald E. Oran J. Shnur R. J. Doyle, Code 6110 Washington, DC 20375	1	Commandant USAFAS ATTN: ATSF-TSM-CN Fort Sill, OK 73503-5600
		1	F.J. Seiler ATTN: S. A. Shackleford USAF Academy, CO 80840-6528
		1	University of Dayton Research Institute ATTN: D. Campbell AL/PAP Edwards AFB, CA 93523

No. of Copies	Organization	No. of Copies	Organization
1	NASA Langley Research Center Langley Station ATTN: G. B. Northam/MS 168 Hampton, VA 23365	1	Cohen Professional Services ATTN: N. S. Cohen 141 Channing Street Redlands, CA 92373
4	National Bureau of Standards ATTN: J. Hastie M. Jacox T. Kashiwagi H. Semerjian US Department of Commerce Washington, DC 20234	1	Exxon Research & Eng. Co. ATTN: A. Dean Route 22E Annandale, NJ 08801
1	Aerojet Solid Propulsion Co. ATTN: P. Micheli Sacramento, GA 95813	1	Ford Aerospace and Communications Corp. DIVAD Division Div. Hq., Irvine ATTN: D. Williams Main Street & Ford Road Newport Beach, CA 92663
1	Applied Combustion Technology, Inc. ATTN: A. M. Varney P.O. Box 607885 Orlando, FL 32860	1	General Applied Science Laboratories, Inc. 77 Raynor Avenue Ronkonkama, NY 11779-6649
2	Applied Mechanics Reviews The American Society of Mechnical Engineers ATTN: R. E. White A. B. Wenzel 345 E. 47th Street New York, NY 10017	1	General Electric Ordnance Systems ATTN: J. Mandzy 100 Plastics Avenue Pittsfield, MA 01203
1	Atlantic Research Corp. ATTN: M. K. King 5390 Cherokee Avenue Alexandria, VA 22314	2	General Motors Rsch Labs Physics Department ATTN: T. Sloan R. Teets Warren, MI 48090
1	Atlantic Research Corp. ATTN: R. H. W. Waesche 7511 Wellington Road Gainesville, VA 22065	2	Hercules, Inc. Allegheny Ballistics Lab. ATTN: W. B. Walkup E. A. Yount P.O. Box 210 Rocket Center, WV 26726
1	AVCO Everett Research Laboratory Division ATTN: D. Stickler 2385 Revere Beach Parkway Everett, MA 02149	1	Alliant Techsystems, Inc. Marine Systems Group ATTN: D. E. Broden/ MS MN50-2000 600 2nd Street NE Hopkins, MN 55343
1	Battelle Memorial Institute Tactical Technolgoy Center ATTN: J. Huggins 505 King Avenue Columbus, OH 43201	1	Alliant Techsystems, Inc. ATTN: R. E. Tompkins MN38-3300 5700 Smetana Drive Minnetonka, MN 55343

44

No. of Copies	Organization	No. of Copies	Organization
1	United Technologies Research Center ATTN: A. C. Eckbreth East Hartford, CT 06108	2	University of California, Santa Barbara Quantum Institute ATTN: K. Schofield M. Steinberg Santa Barbara, CA 93106
3	United Technologies Corp. Chemical Systems Division ATTN: R. S. Brown T. D. Myers (2 copies) P.O. Box 49028 San Jose, CA 95161-9028	1	University of Colorado at Boulder Engineering Center ATTN: J. Daily Campus Box 427 Boulder, CO 80309-0427
1	Universal Propulsion Company ATTN: H. J. McSpadden Black Canyon Stage 1 Box 1140 Phoenix, AZ 85029	2	University of Southern California Dept. of Chemistry ATTN: S. Benson C. Wittig Los Angeles, CA 90007
1	Veritay Technology, Inc. ATTN: E. B. Fisher 4845 Millersport Highway P.O. Box 305 East Amherst, NY 14051-0305	1	Cornell University Department of Chemistry ATTN: T. A. Cool Baker Laboratory Ithaca, NY 14853
1	Brigham Young University Dept. of Chemical Engineering ATTN: M. W. Beckstead Provo, UT 84058	1	University of Delaware ATTN: T. Brill Chemistry Department Newark, DE 19711
1	California Institute of Tech. Jet Propulsion Laboratory ATTN: L. Strand, MS 512/102 4800 Oak Grove Drive Pasadena CA, 91109	1	University of Florida Dept. of Chemistry ATTN: J. Winefordner Gainesville, FL 32611
1	California Institute of Technology ATTN: F. E. C. Culick/MC 301-46 204 Karman Lab. Pasadena, CA 91125	3	Georgia Institute of Technology School of Aerospace Engineering ATTN: E. Price W. C. Strahle B. T. Zinn Atlanta, GA 30332
1	University of California Los Alamos Scientific Lab. P.O. Box 1663, Mail Stop B216 Los Alamos, NM 87545	1	University of Illinois Dept. of Mech. Eng. ATTN: H. Krier 144MEB, 1206 W. Green Street Urbana, IL 61801
1	University of California, Berkeley Chemistry Department ATTN: C. Bradley Moore 211 Lewis Hall Berkeley, CA 94720		
1	University of California, San Diego ATTN: F. A. Williams AMES, B010 La Jolla, CA 92093		

No. of Copies	Organization	No. of Copies	Organization
1	Johns Hopkins University/APL Chemical Propulsion Information Agency ATTN: T. W. Christian Johns Hopkins Road Laurel, MD 20707	2	Purdue University School of Mechanical Engineering ATTN: N. M. Laurendeau S. N. B. Murthy TSPC Chaffee Hall West Lafayette, IN 47906
1	University of Michigan Gas Dynamics Lab Aerospace Engineering Lab ATTN: G. M. Faeth Ann Arbor, MI 48109-2140	1	Rensselaer Polytechnic Inst. Dept. of Chemical Engineering ATTN: A. Fontijn Troy, NY 12181
1	University of Minnesota Dept. of Mechanical Engineering ATTN: E. Fletcher Minneapolis, MN 55455	1	Stanford University Dept. of Mechanical Engineering ATTN: R. Hanson Stanford, CA 94305
3	Pennsylvania State University Applied Research Laboratory ATTN: K. K. Kuo H. Palmer M. Micci University Park, PA 16802	1	University of Texas Dept. of Chemistry ATTN: W. Gardiner Austin, TX 78712
1	Pennsylvania State University Dept. of Mechanical Engineering ATTN: V. Yang University Park, PA 16802	1	University of Utah Dept. of Chemical Engineering ATTN: G. Flandro Salt Lake City, UT 84112
1	Polytechnic Institute of NY Graduate Center ATTN: S. Lederman Route 110 Farmingdale, NY 11735	1	Virginia Polytechnic Institute and State University ATTN: J. A. Schetz Blacksburg, VA 24061
2	Princeton University Forrestal Campus Library ATTN: K. Brezinsky I. Glassman P.O. Box 710 Princton, NJ 08540	1	Freedman Associates ATTN: E. Freedman 2411 Diana Road Baltimore, MD 21209-1525
1	Purdue University School of Aeronautics and Astronautics ATTN: J. R. Osborn Grissom Hall West Lafayette, IN 47906		
1	Purdue University Department of Chemistry ATTN: E. Grant West Lafayette, IN 47906		

USER EVALUATION SHEET/CHANGE OF ADDRESS

This Laboratory undertakes a continuing effort to improve the quality of the reports it publishes. Your comments/answers to the items/questions below will aid us in our efforts.

1. BRL Report Number ____BRL-TR-3204____ Date of Report ____February 1991____

2. Date Report Received _____

3. Does this report satisfy a need? (Comment on purpose, related project, or other area of interest for which the report will be used.) _____
_____
_____

4. Specifically, how is the report being used? (Information source, design data, procedure, source of ideas, etc.) _____
_____
_____

5. Has the information in this report led to any quantitative savings as far as man-hours or dollars saved, operating costs avoided, or efficiencies achieved, etc? If so, please elaborate. _____
_____
_____

6. General Comments. What do you think should be changed to improve future reports? (Indicate changes to organization, technical content, format, etc.) _____
_____
_____
_____

CURRENT
ADDRESS

| Name |
| Organization |
| Address |
| City, State, Zip Code |

7. If indicating a Change of Address or Address Correction, please provide the New or Correct Address in Block 6 above and the Old or Incorrect address below.

OLD
ADDRESS

| Name |
| Organization |
| Address |
| City, State, Zip Code |

(Remove this sheet, fold as indicated, staple or tape closed, and mail.)

--FOLD HERE--

DEPARTMENT OF THE ARMY
Director
U.S. Army Ballistic Research Laboratory
ATTN: SLCBR-DD-T
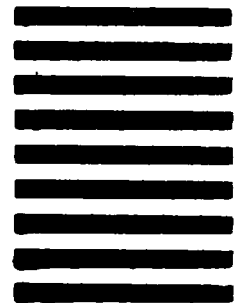Aberdeen Proving Ground, MD 210(-5066
    OFFICIAL BUSINESS

BUSINESS REPLY MAIL
FIRST CLASS PERMIT No 0001, APG, MD

POSTAGE WILL BE PAID BY ADDRESSEE

Director
U.S. Army Ballistic Research Laboratory
ATTN: SLCBR-DD-T-
Aberdeen Proving Ground, MD 21005-9989

--FOLD HERE--